THE CRYSTAL CHEMISTRY OF MTO_4 COMPOUNDS WITH THE ZIRCON, SCHEELITE, AND MONAZITE STRUCTURE TYPES

by

Brett Jarrod Macey

Thesis submitted to the Faculty of the

Virginia Polytechnic Institute and State University

in partial fulfillment of the requirements for the degree of

MASTER OF SCIENCE

in

Geological Sciences

APPROVED:

P. H. Ribbe, Chairman

G. V. Gibbs

R. J. Bodnar

September, 1995

Blacksburg, Virginia

THE CRYSTAL CHEMISTRY OF MTO_4 COMPOUNDS WITH THE ZIRCON, SCHEELITE, AND MONAZITE STRUCTURE TYPES

by

Brett Jarrod Macey

P. H. Ribbe, Chairman

Department of Geological Sciences

(ABSTRACT)

The crystal structures of zircon, scheelite, and monazite are very closely related. All three have chains of alternating polyhedra and planes of closest packed or pseudo-closest packed cations. Using these similarities the unit cells of these structures can be placed in analogous orientations. This in turn leads to a better understanding of the geometrical aspects of the reconstructive phase transformations that occur among the structure types as functions of temperature and pressure. In essence the phase transformations require the cation planes of one structure to the cation planes of another. Phase transformations also occur via compositional pathways.

Crystal structure parameters were modeled for compounds with the zircon, scheelite and monazite structure types using multiple regression techniques. Data consisted of structure refinements of 26 zircon-, 13 scheelite-, and 13 monazite-type compounds. These compounds include but are not limited to the lanthanide vanadates and phosphates, the alkali earth molybdates and tungstates, and $KTcO_4$. The structural parameters studied included bond lengths, bond angles, polyhedral volumes, unit cell edge lengths, tetrahedral quadratic elongations and atomic coordinates of individual atoms; they were modeled as a function of the Shannon radii of the cations and the product of the M and T cation charges. Correlation coefficients for these regressions exceeded 0.9 for nearly all parameters studied except for the y coordinate of M, the z coordinate of O1, and T-O1-M2 angle of the monazite compounds.

Acknowledgments

I thank A. K. Sinha for proposing the idea that eventually lead to this project. Jerry Gibbs helped me through a number of difficulties as well as putting one or two in my way! Bob Bodnar pointed out the necessity of validating my work not only to the scientific community but to the community in general. I thank him for his practicality, which I sometimes lack. Most of all I wish to thank Paul Ribbe. Paul has been a constant source of encouragement and good advice over the five years which I have known him.

Table of Contents

List of Tables

List of Figures

Preface

MTO_4 compounds with the zircon-, monazite-, and scheelite-type structures have many uses to the geologic and materials science communities. The mineral zircon is of great importance because of its usefulness in geochronology. It is also a refractory mineral, able to withstand high pressures and temperatures as well as mechanical and chemical breakdown. Compounds with this structure type have low thermal expansions making them useful in the ceramics industry (Muller and Roy, 1974). The zircon-type mineral xenotime (YPO_4) is a primary source of the rare earth element yttrium. Compounds with the monazite-type structure can accept large actinide and lanthanide cations and have therefore been investigated as a possible repository for high-level radioactive waste storage (Aldred, 1984). The mineral monazite itself is a primary source of the element thorium. Compounds with the scheelite-type structure can be used in lasers when doped with lanthanide elements (Muller and Roy, 1974). With the regression equations developed in this study it is possible to obtain structural parameters for hypothetical compounds with the zircon-, monazite-, and scheelite-type structures from the radii of the cations and the product of their charges.

INTRODUCTION

There is considerable geologic interest in compounds of the MTO_4 type, especially the mineral zircon. Zircon is important in geochronology because it often contains uranium, thorium, and their decay products. Reid and Ringwood (1969) found that $(ZrSiO_4)_Z$ transforms to a scheelite-type structure, $(ZrSiO_4)_S$, under static and shock compression. Over a certain pressure range not all of the $ZiSiO_4$ is converted to the high pressure phase, and there is interest in attempting to use shocked zircons as indicators of meteorite impact pressures (Ribbe and Macey, 1994). To this date, however, no shocked $ZrSiO_4$ has been found in nature with the scheelite-type structure. An attempt to understand the zircon $\Rightarrow$ scheelite transformation led to an exploration of zircon- and scheelite-type structures for a variety of compositions (Muller and Roy, 1974). It was found that phase transformations between these structure-types are not at all uncommon and that the structures themselves are very closely related to each other and to the monazite-type structure (Muller and Roy, 1974).

With this in mind, a study was undertaken to accomplish three goals: to compare and contrast the three structure types, to determine the geometrical aspects of structural transformations with changes in pressure and temperature from one structure type to another, and to determine the effects of M and T cation substitutions on the structures and their stability fields.

STRUCTURE DISCRIPTIONS AND STRUCTURAL ANALOGIES

Zircon

The structure of zircon ($ZrSiO_4$) was independently determined by Vegard (1926), by Binks (1926), and by Hassel (1926). Zircon crystallizes with space group $I4_1/amd$ and its unit cell contains 4 metal cations (hereafter referred to as M cations), 4 tetrahedrally-coordinated cations (referred to as T cations), and 16 oxygens. The cations lie on

Wyckoff positions 4a for Zr and 4b for Si (x, y, and z fixed for both) while oxygen lies on 16h (fixed x coordinate). The zircon structure consists of isolated tetrahedral groups and larger eight-coordinated M polyhedra (see Fig.1). Each tetrahedron shares two opposite edges with adjacent triangular dodecahedra. These alternating dodecahedra and tetrahedra form chains that are parallel to [001] (see Fig.1). The tetrahedra are among the most distorted of known silicates, having quadratic elongations of 1.024 and angle variances (from the ideal 109.4°) of 97.31° (Robinson, et. al., 1971). They are elongate along c and the T-O distances are equivalent, making them tetragonal disphenoids. Each dodecahedron shares 4 edges with adjacent dodecahedra and 2 edges with adjacent tetrahedra.

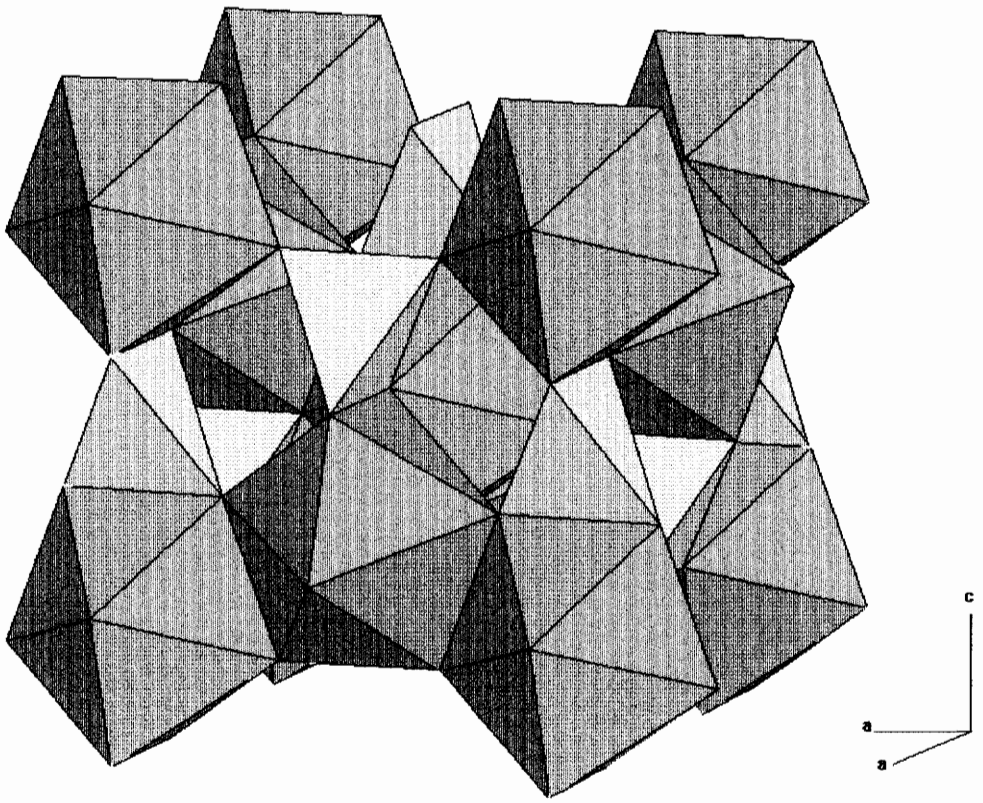

Figure 1. Polyhedral representation of zircon. Note the chains of edge-sharing alternating dodecahedra and tetrahedra running along **c**.

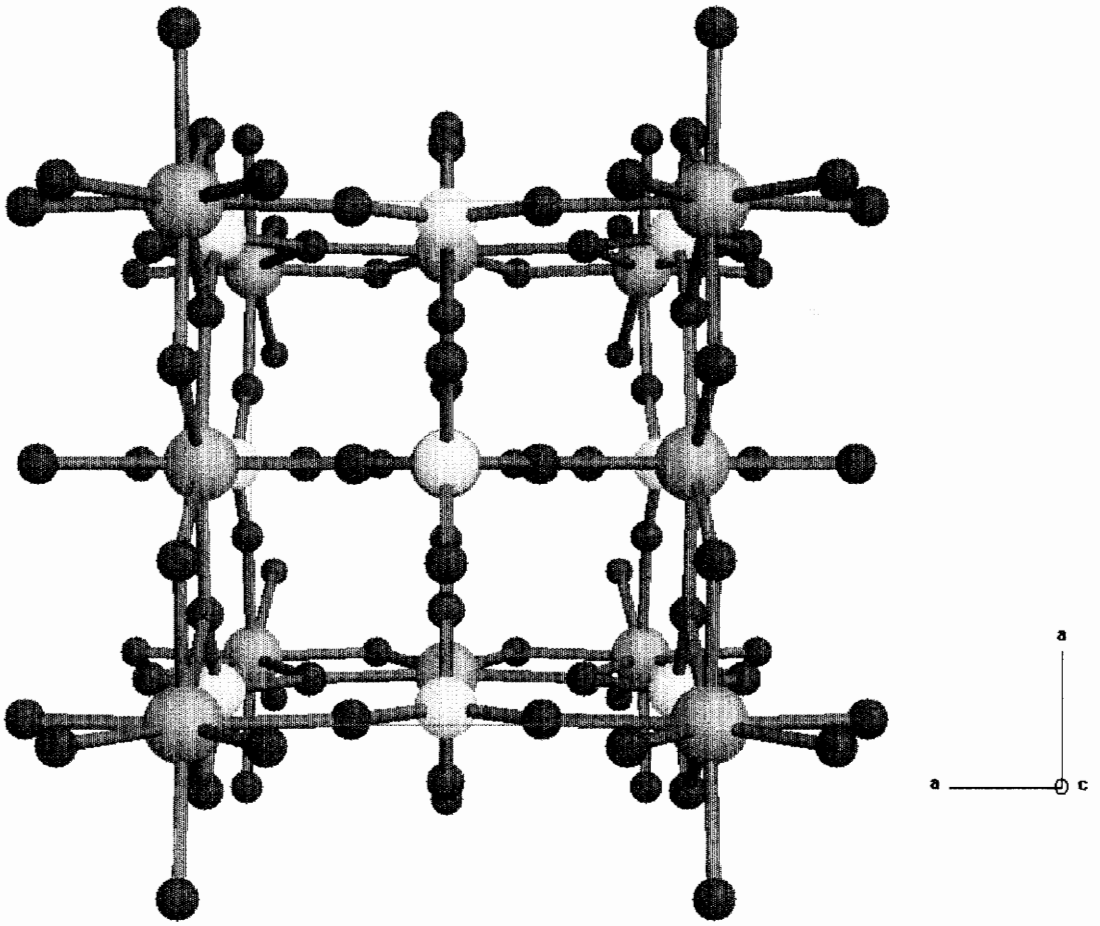

Figure 2. Atomic representation of zircon. Small dark spheres are oxygens, medium white spheres are Si, and large grey spheres are Zr. View is down [100].

Considering the zircon structure in terms of atoms instead of polyhedra, it can be seen that it consists of two equivalent sets of planes which contain all the M, T, and O atoms. These planes, (100) and (010), form square 'channels' along [001] (see Fig. 2). They are composed of oxygens, each coordinated to one T cation and two M cations.

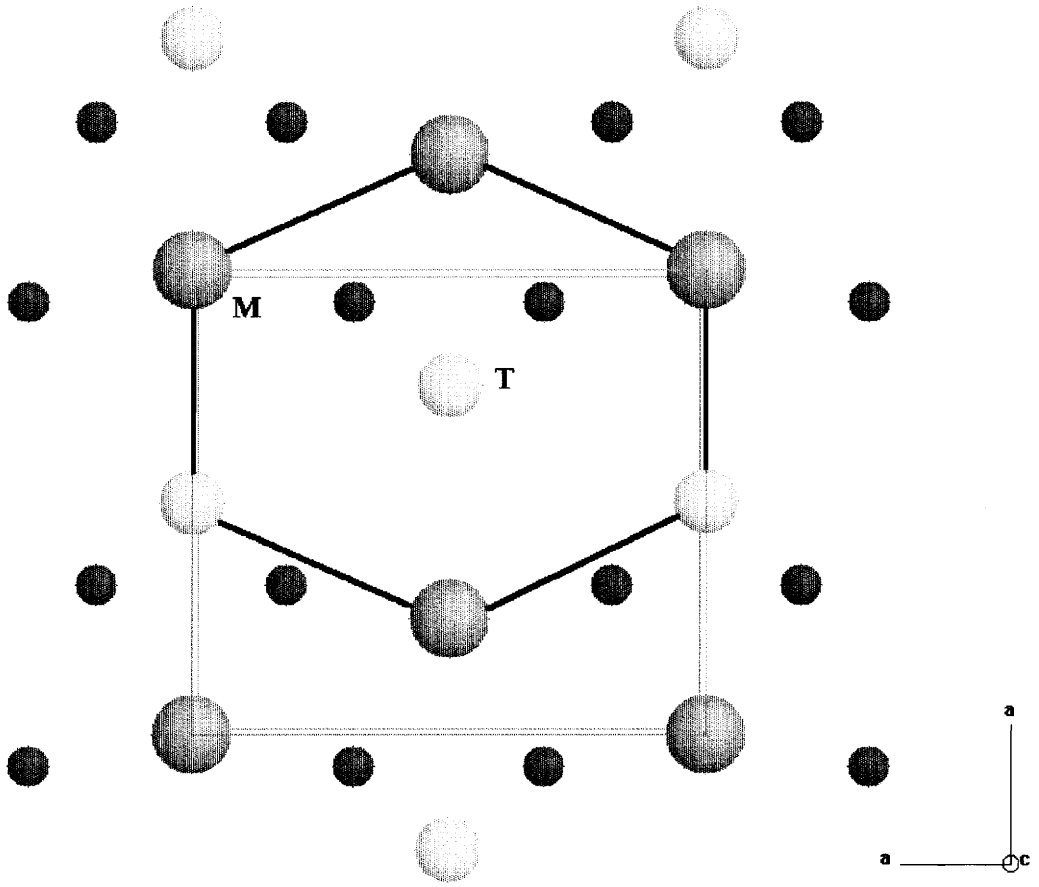

Figure 3. Atoms of the (100) of zircon. Atom represenatations are the same as in Figure 2.

The M1-M2 and M2-T distances are equal (Fig. 3). As pointed out by O'Keeffe and Hyde (1985), the (100) and (010) planes also have pseudo-closest packing of cations.

Monazite

Kokkoros (1942) first solved the monazite ($CePO_4$) structure and gave it the non-standard space group of $P2_1/n$. For the purposes of this paper $P2_1/n$ has been transformed to the standard space group $P2_1/c$ by the following 3x3 matrix:

$$\begin{matrix} 0 & 0 & 1 \\ \underline{0} & 1 & 0 \\ 1 & 0 & 1 \end{matrix}$$

The unit cell contains 4 M cations, 4 T cations, and 16 oxygens. All of the atoms lie on general positions (Wyckoff positions 4e). The structure consists of 9-coordinated M

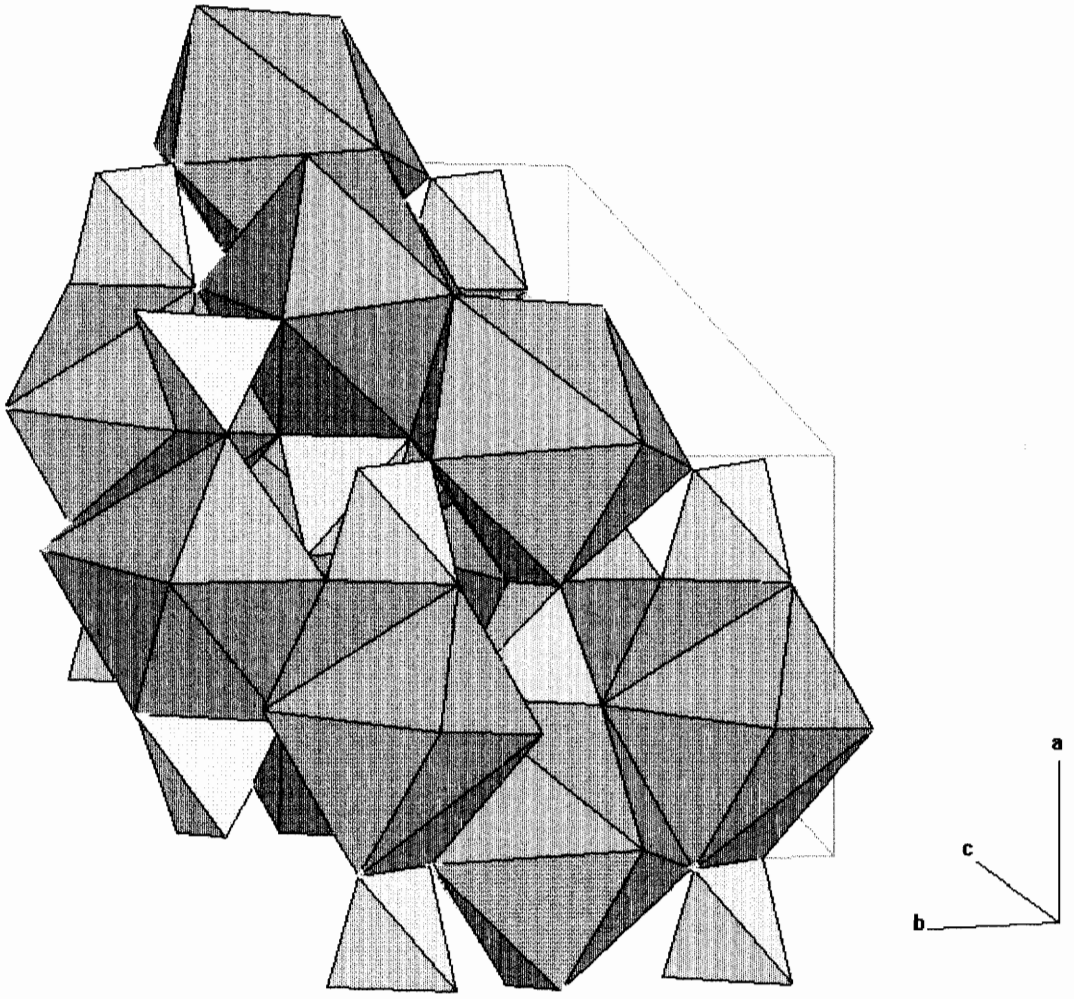

Figure 4. Polyhedral representation of monazite. Note the alternating edge-sharing polyhedral chains parallel to **a**.

polyhedra and isolated tetrahedra. Their linkages are similar to that in the zircon structure (see Fig. 4, compare with Fig. 1). The tetrahedra share opposite edges with M polyhedra, alternating to form chains. These parallel chains differ from those in zircon in that they are not as straight; the polyhedra are slightly rotated and displaced (see Fig. 4). The linkages among the M polyhedra are also different due to the higher coordination. Each large polyhedron shares 5 edges with adjacent large polyhedra and 2 with tetrahedra.

The ninth-coordinated oxygen is slightly more distant from the metal cation than the other oxygens leading various researchers to assign the M cation coordinations from eight to ten (Effenberger and Pertlik, 1986). This coordination debate is similar to the one concerning the M2 sites found in certain pyroxenes (Griffen, 1992). The ninth oxygen has an important place in the monazite structure because it forms one of the shared edges with a tetrahedron (see Fig. 5). The T-O bond to this oxygen is longer than the other T-O bonds. Also, the length of the shared edge formed with the ninth oxygen is longer than the opposite shared edge formed with shorter M-O and T-O bonds (see Fig. 5).

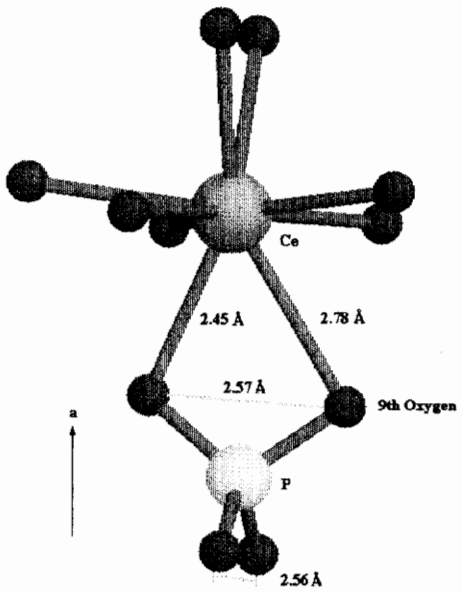

Figure 5. Shared polyhedral edge in monazite containing the ninth coordinated oxygen.

Because monazite and zircon are so similar and because phase transformations occur between compounds with these structure types, one can use the M polyhedral rings and the polyhedral chains to place the unit cells of zircon and monazite in analogous orientations. The polyhedral chains run in the [100] direction in monazite. Thus if the monazite chains are equivalent to the zircon chains then [100]m is analogous to [001]z (compare Fig. 4 and Fig. 1). Knowing one analogous direction, the cation packing of monazite can be compared to that of zircon. The plane of cations parallel to (001) in monazite has a pseudo-hexagonal arrangement, making it a likely analog to (100) of zircon (Fig. 6, compare with Fig. 3). There are no other hexagonal packed planes in the proper orientation (parallel to the polyhedral chains) that could correspond to the zircon (010). Thus $(010)_Z$ most likely becomes a plane parallel to $(010)_M$ (Fig. 7).

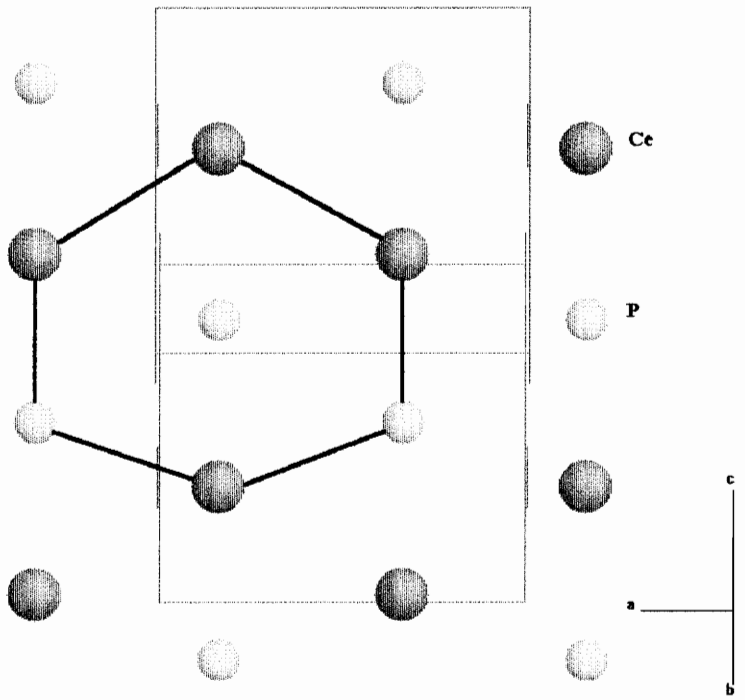

Figure 6. Cation plane of monazite parallel to (001).

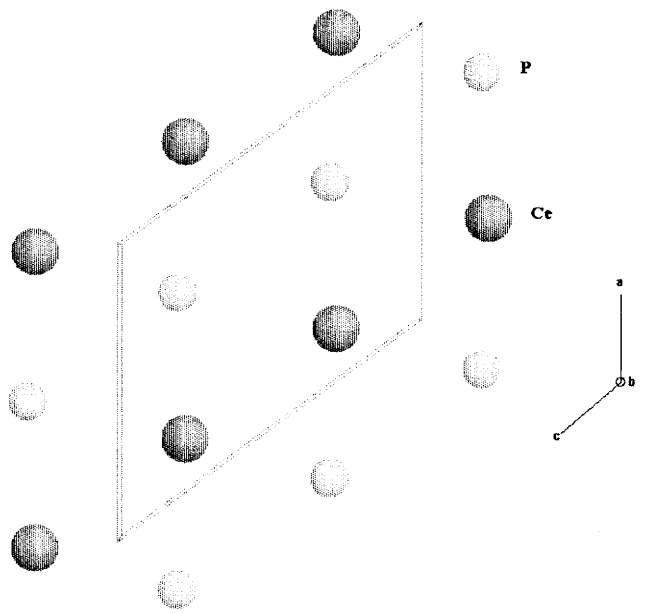

Figure 7. Cations of the plane parallel to (010) in monazite.

The coordinations of the oxygens vary in the monazite structure. There are 4 unique oxygens, 3 of them being 3-coordinated and the other 4-coordinated (this oxygen is the ninth of the large coordination polyhedron). The 3-coordinated oxygens are similar to those in zircon (bonded to 2 M and 1 T). The other oxygen is bonded to 3 M and 1 T; it is over-bonded while the others are equally under-bonded. The degree of over-bonding is a function of the M and T cation charge combination. In huttonite ($ThSiO_4$; +4,+4) the sum of the Pauling bond strengths (Pauling, 1929) reaching the four-coordinated oxygen is 2.33. In $LaPO_4$ (+3,+5) it is 2.25, and in $SrCrO_4$ (+2,+6) it is 2.17.

Scheelite

Scheelite ($CaWO_4$) crystallizes in the space group $I4_1/a$. The structure was first refined by Sillen and Nylander (1943). As with zircon and monazite, the unit cell

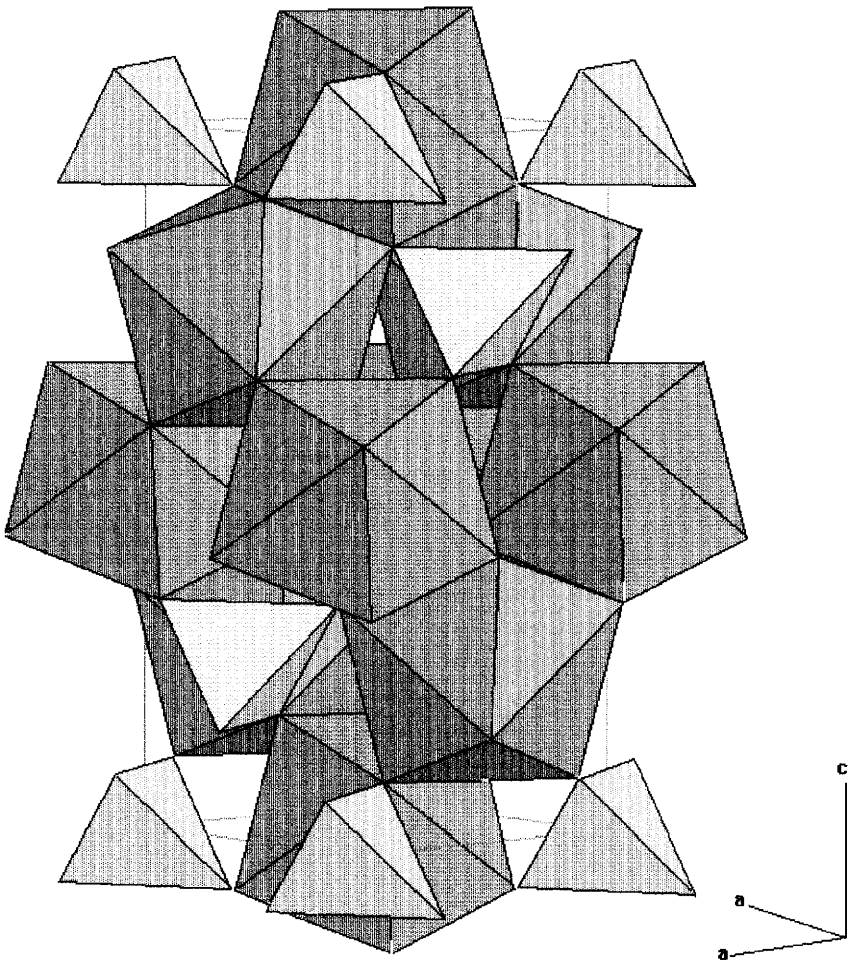

Figure 8. Polyhedral representation of scheelite. Note the corner-sharing between dodecahedra and tetrahedra.

contains 4 M cations , 4 T cations, and 32 oxygens. The M and T cations both lie on special positions (Wyckoff positions: Ca on 4b and W on 4a) and the oxygen occupies a general position (Wyckoff position 16f). Scheelite differs from zircon and monazite in that the TO_4 polyhedra share four vertices with adjacent dodecahedra (see Fig. 8). Thus chains of alternating edge-sharing polyhedra do not exist.

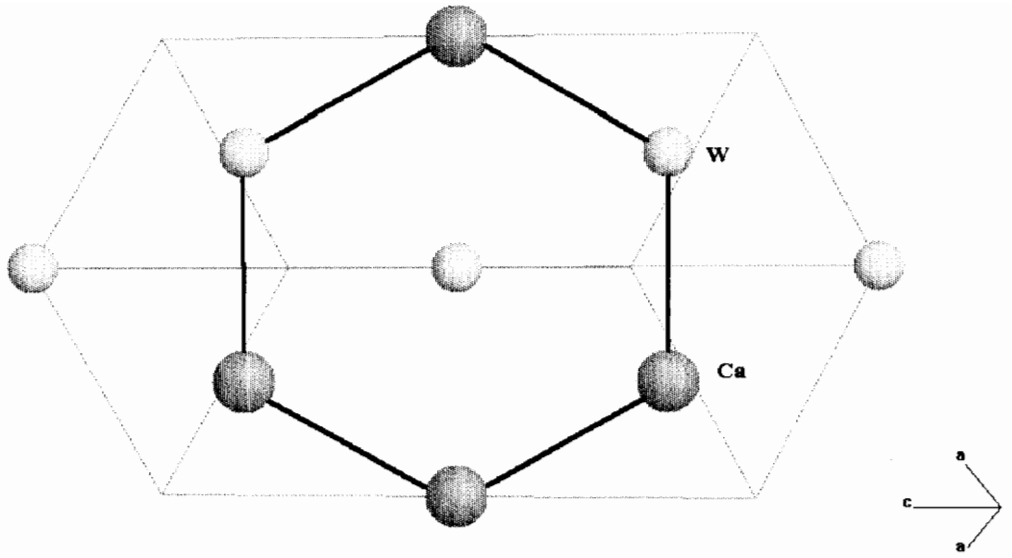

Figure 9. The cations of the (112) plane of scheelite.

The cation packing of scheelite is very nearly cubic closest packed, as O'Keeffe and Hyde (1985) have noted, paralleling {112} (see Fig. 9). Oxygens occupy the tetrahedral interstices, however, they do not lie at the centers of the OT_2M_2 tetrahedra. In fact, the oxygens are three-coordinated to two M cations and one T cation with the arrangement being nearly planar (as in zircon; cf. Fig. 12 below). Bayer (1978) noted that the [110] of scheelite is analogous to [001] of zircon With this in mind one can see that the {112} closest packed cation planes of scheelite are analogous to the {100} pseudo-closest packed cation planes of zircon (compare Fig. 9 with Fig. 3). Scheelite has chains of alternating corner-sharing tetrahedra and dodecahedra that are parallel to [110]s which is analogous to [001]z and thus parallel to the edge-sharing polyhedral chains of zircon. Because the monazite polyhedral chains are analogous to those of zircon they must also be analogous to those of scheelite as clearly shown Fig. 10.

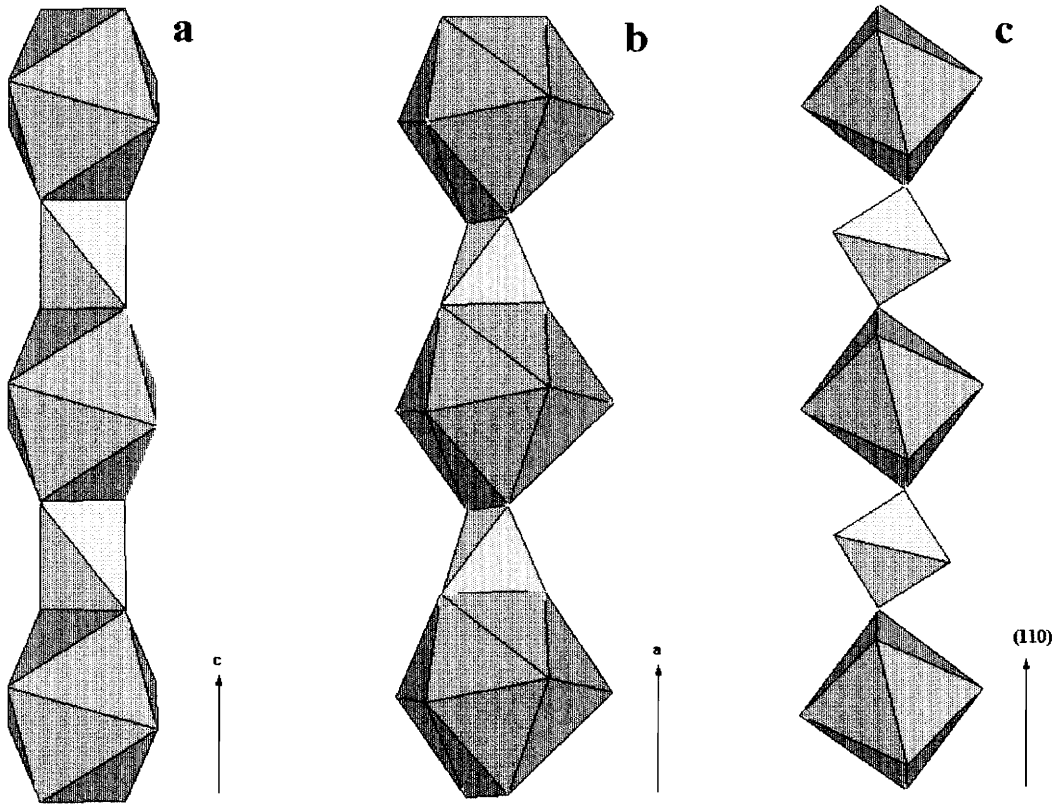

Figure 10. Portions of polyhedral chains from (a) zircon, (b) monazite, and (c) scheelite.

STRUCTURAL PHASE TRANSFORMATIONS

The Zircon ⇒ Scheelite Transformation

There has been some confusion regarding the nature of the transformation of zircon-type compounds to the scheelite-type compounds. Knittle and Williams (1993) proposed a "low temperature diffusional pathway" while Kusaba et. al. (1984) have called the transformation "displacive." It will be shown that the transformation is reconstructive in nature. The evidence is two-fold: first, the transformed product is metastable (Knittle and Williams, 1993). This in turn suggests that a kinetic energy barrier prevents the transformed product from reverting to its former state. In a displacive

transformation no such barrier exists. Only small displacements of atoms are necessary in a displacive transformation (no bonds are broken); therefore, no substansial kinetic energy barrier exits to prevent a reversion to the original state. In short, displacive transformations are not quenchable, the transformed products are not stable (Griffen, 1992). Because $(ZrSiO_4)_S$ is metastable, this suggests that bonds have been broken and new ones established. This is easily observed. In the zircon structure, tetrahedra share two opposite edges with adjacent dodecahedra. In the scheelite structure they share four corners with adjacent dodecahedra. The change from edge-sharing to corner-sharing must be reconstructive.

Although much interest lies in the $(ZrSiO_4)_Z \Rightarrow (ZrSiO_4)_S$ transformation, the geometrical aspects of the transformation we first studied using the $ThGeO_4$ polymorphs (Ribbe and Macey, 1994). But in this thesis $ErVO_4$ was studied instead. All of the vanadates and arsenates with zircon-type structure undergo transformations to scheelite-type structures with sufficient pressure (Stubican and Roy, 1963). The crystal structure of $(ZrSiO_4)_S$ has not been refined (except crudely by the Reitveld method) despite the many investigations of the transformation: Kusaba, et. al. (1984), Mashimo, et. al. (1983), Kusaba, et. al. (1986), and Knittle and Williams (1993).

$ErVO_4$ crystallizes with the zircon structure at STP. With high pressure and temperature (35 kbar and 1500K) it transforms to a scheelite-type structure (Range and Miester, 1990). The $(ErVO_4)_Z \Rightarrow (ErVO_4)_S$ transformation involves changing the pseudo-closest packed planes in zircon to the closest packed planes in scheelite. The cation planes of zircon, (100) and (010), are orthogonal. The {112} cation planes {112} in $(ErVO_4)_S$ intersect at 64.83° (see Fig. 11a, 11b). Thus the transformation involves shearing along {100} of the zircon structure. This mechanism brings {100} planes from a distance of 3.55 Å to 2.99 Å from each other. It is necessary to bring the cation planes closer together to attain closest packing. This mechanism decreases the volume of the unit cell drastically: $(ErVO_4)_Z$ has a cell volume of 315.83 $Å^3$ while

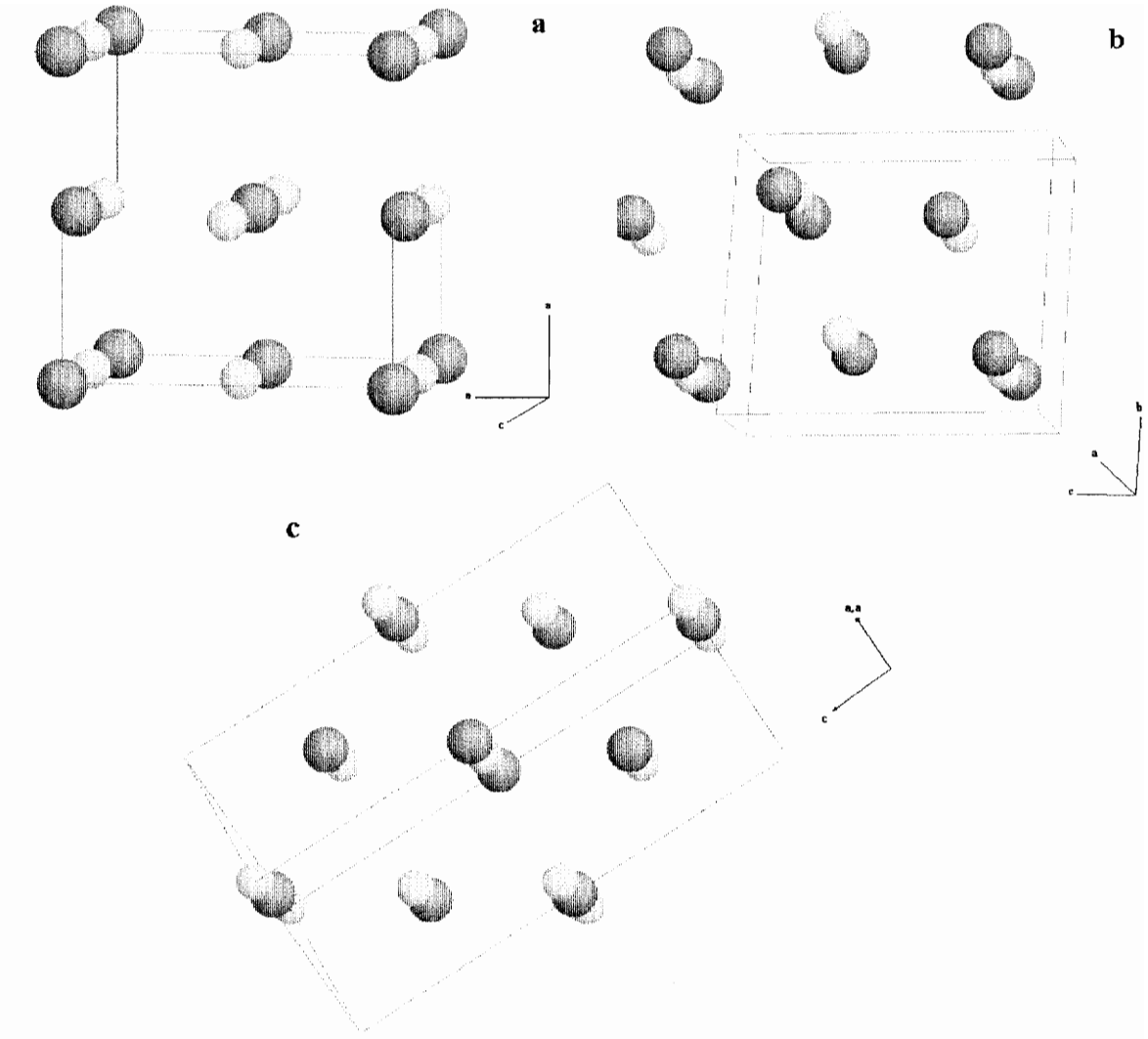

Figure 11. Cation representations of (a) zircon, (b) monazite, and (c) scheelite. The unit cells of monazite and scheelite have been chosen to be analogous with the unit cell of zircon.

$(ErVO_4)_S$ has a volume of 278.91 $Å^3$, a decrease of 11.8%. Along with the shearing, a slight distortion must occur within the cation planes of the zircon structure to attain the closest packing of the scheelite structure (see Fig. 11a and 11c). No change in primary coordination is necessary for the transformation to take place.

There is actually little change in bond lengths as result of the transformation. The two unique M-O bonds become more equal going from 2.28 Å and 2.43 Å in $(ErVO_4)_Z$ to 2.33 Å and 2.37 Å in $(ErVO_4)_S$. The dodecahedral volume shrinks slightly from 23.44 $Å^3$ to 23.09 $Å^3$. The T-O distances may increase or decrease slightly. Two structure refinements of $(ErVO_4)_Z$ give different V-O distances. Patscheke et al (1968) report a V-O distance of 1.72 Å while Chakoumakos et al (1994) give a V-O distance of 1.71 Å. The V-O distance in the scheelite form is 1.72 Å (Range and Miester, 1990), thus the T-O distance either drops slightly or stays the same. The mean tetrahedral quadratic elongation drops from 1.013 to 1.010. The reason for this can be found in the M-T distances along the polyhedral chain. The Er1···V distance (where Er1 and V are cations in the same chain and Er2 is the nearest cation of the adjacent chain) in the zircon modification is very short at 3.14 Å (Fig. 12a). In the scheelite structure it increases to 3.54 Å which is comparable to the other cation-cation distances Er2···V and Er1···Er2 of 3.74 Å (Figure 12c). With the increase of the Er1···V distance, the strong M···T cation repulsions are reduced, thus reducing the tetrahedral distortions.

O'Keeffe and Hyde (1981) have used non-bonded interactions to explain such changes. The scheelite structure consists of closest packed cations. If we assume that the cations are in non-bonded contact (i.e., that the cations are large while the anions are small), some interesting conclusions may be drawn. In a structure with cations in closest packing and in contact, the cation-cation distances should be equal. Because we are dealing with two cations that differ significantly in size, we should expect the cation-cation distances to be close but not equal. This is exactly what is observed in the scheelite structure. In the zircon structure the M···T distance along the polyhedral chain is much shorter than the other cation-cation distances. O'Keeffe and Hyde (1985) have stated that decreasing the distance between two cations to less than the sum of their non-

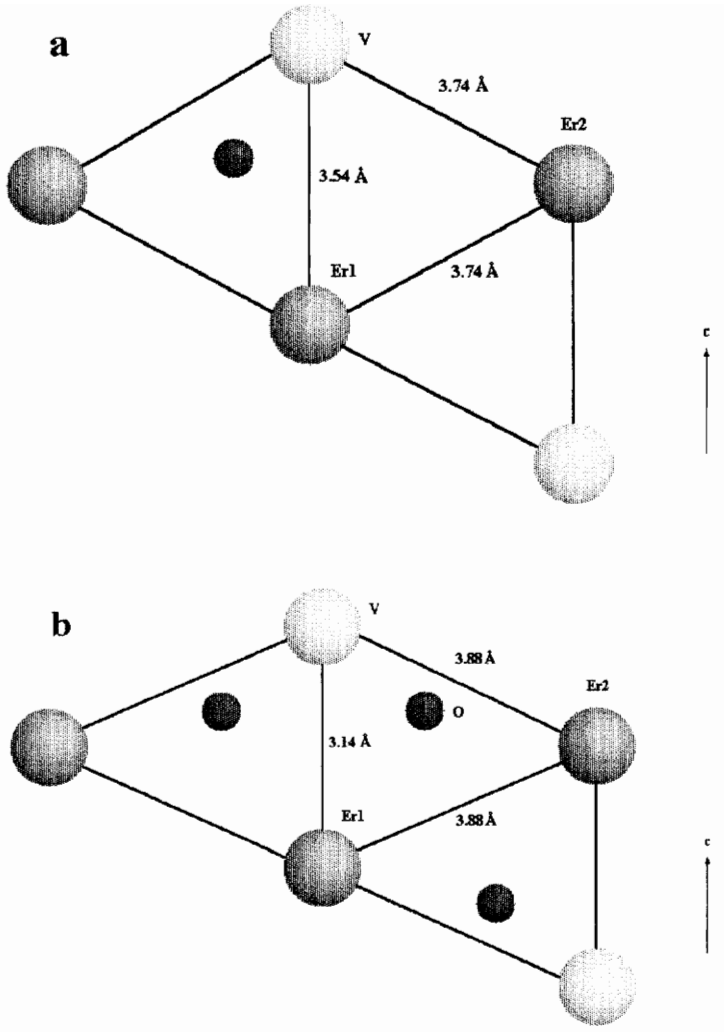

Figure 12. Portions of (a) the (100) of $(ErVO_4)_Z$ and (b) the (112) of $(ErVO_4)_S$.

bonded radii can have one of two effects: the first may be a reduction of coordination of the cation (such as the diamond/graphite transformation), the second may be a change from corner-sharing polyhedra to edge-sharing polyhedra. In other words, the two close cations share two bridging anions, with two sets of bonds between them to accommodate the increased electrostatic repulsion.

Let us examine the $ErVO_4$ polymorphs and attempt to verify one of these results. The non-bonded radius of vanadium is not given by O'Keeffe and Hyde (1985) but by modeling their data as a function of the Shannon radii (an equation of the form non-bonded radius = A(Shannon radius) + a constant) we may estimate the radius at 1.56 Å. No radius is given for erbium, but we may derive our own. The Er1···Er2 distance in the scheelite form is 3.54 Å (Fig. 12b). Because we have assumed that the cations are in contact, we may assume that the Er1···Er2 distance is twice the erbium non-bonded radius (i.e., Er = 1.77 Å). Therefore, the optimum Er1···V distance should be the sum of these two radii: 3.33 Å. In the zircon modification the closest Er1···V distance is 3.14 Å (Fig. 15a), clearly smaller than the sum of the non-bonded radii. Thus, due to strong cation repulsions another set of bonds are formed between the two close cations resulting in a change from corner-sharing to edge-sharing. The non-bonded interaction of Er and V also accounts for the larger distortions of the VO_4 tetrahedron (in the zircon modification), which is elongated in the direction of the chain, the direction in which the shortest cation-cation distances are found.

Figure 13. The univarient P-T curve for the $(HoVO_4)_Z \Rightarrow (HoVO_4)_S$ transformation.

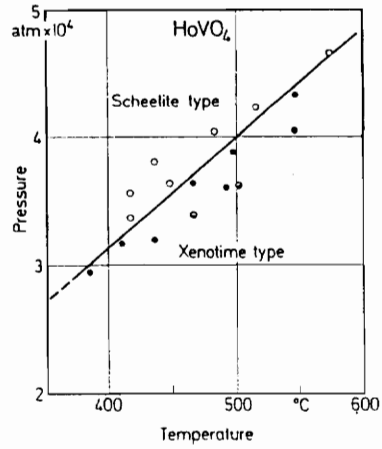

Stubican and Roy (1963) found that the univariant pressure-temperature curve for the zircon ⇒ scheelite transformation has a positive slope (Fig. 13). This indicates that the transformation occurs via a pressure pathway. It also indicates that temperature

should cause the reverse transformation scheelite ⇒ zircon. This transformation has been observed in some of the actinide germanates ($PaGeO_4$, $UGeO_4$, $ThGeO_4$, and $NpGeO_4$) (Keller, 1963). Structure refinements on the polymorphic pairs of $ThGeO_4$ (Vandenborre, et. al., 1989) show the transformation to be virtually the same as the zircon ⇒ scheelite transformation (see Table 1).

Table 1. Structural parameters of the $ThGeO_4$ polymorphs

Compound	T vol, Å^3	T-O, Å	TQE*	M1-O, Å	M2-O, Å	M vol, Å^3	M···T, Å	Vol, Å^3
α-$ThGeO_4$	2.551	1.731	1.028	2.332	2.352	23.051	3.638	278.77
β-$ThGeO_4$	2.646	1.750	1.026	2.358	2.473	25.290	3.270	341.81

*Tetrahedral quadratic elongation, as defined by Robinson, Gibbs, and Ribbe (1971)

α = Scheelite-type structure

β = Zircon-type structure

The Zircon ⇒ Monazite Transformation

This transformation seldom has been observed. It is known to occur in only a few compounds such as $ThSiO_4$, $PaSiO_4$, and $CeVO_4$. Temperature appears to be responsible for the zircon ⇒ monazite transformation, but Mumpton and Roy (1961) suggested that $(ThSiO_4)_Z$ (thorite) is the metastable phase. Keller (1963), however, found that both $ThSiO_4$ and $PaSiO_4$ transform from the zircon- to the monazite-type structure at temperatures of about 1200°C, and Range, et. al. (1990) found that $CeVO_4$ transforms to the monazite structure at about 1300°C at atmospheric pressure (Fig. 17). The transformation involves a decrease in density less than that of the zircon ⇒ scheelite, but is substantial nonetheless (about 8%). It involves a reduction of symmetry from $I4_1/amd$ to $P2_1/c$. Also, the transformation is reconstructive in nature. This is easily seen by the fact the transformed products are metastable (Range, et. al., 1990). Also with the addition of a ninth oxygen to the M-coordination sphere, new bonds are formed, providing a kinetic energy barrier preventing reversion.

Figure 14. T-P phase diagram of the $CeVO_4$ polymorphs.

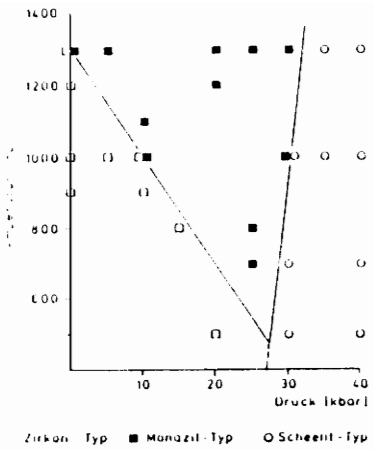

Unlike zircon ⇒ scheelite, the zircon ⇒ monazite transformation does not seem to require a simple shear to take place. The (100) and (010) planes of zircon are transformed to the cation planes parallel to (001) and (010) of monazite (Fig. 14a and Fig. 14c). Because these two planes in monazite are orthogonal, no shearing is required.

Details of the transformation were acquired by study of the $ThSiO_4$ polymorphs thorite and huttonite (Taylor and Ewing, 1978). As mentioned earlier, the transformation is accompanied by a reduction in volume from 321.48 $Å^3$ in thorite to 297.14 $Å^3$ in huttonite. Interestingly, the large cation polyhedron increases in size from thorite (25.32 $Å^3$) to huttonite (30.41$Å^3$). Part of this is due to the fact that the large cations in huttonite are 9-coordinated while those in thorite are 8-coordinated. If the ninth oxygen of huttonite is discounted, the volumes of the MO_8 polyhedra in the two structures are nearly equal (thorite = 25.32 $Å^3$, huttonite = 25.49 $Å^3$). The SiO_4 tetrahedra change little in volume from 2.21 $Å^3$ in thorite to 2.12 $Å^3$ in huttonite. With the cation polyhedra changing so little, the volume decrease must come from the collapse of vacant "polyhedra". The four unique T-O bond lengths are on the average shorter in huttonite (1.64 Å to 1.58 Å, average = 1.62 Å) than in thorite (all 1.63 Å). Both the shared edge lengths in thorite are 2.52 Å (Fig. 18). In huttonite one shared edge is slightly longer at 2.54 Å and the other smaller at 2.46 Å. This is interesting because the Th1···Si distance

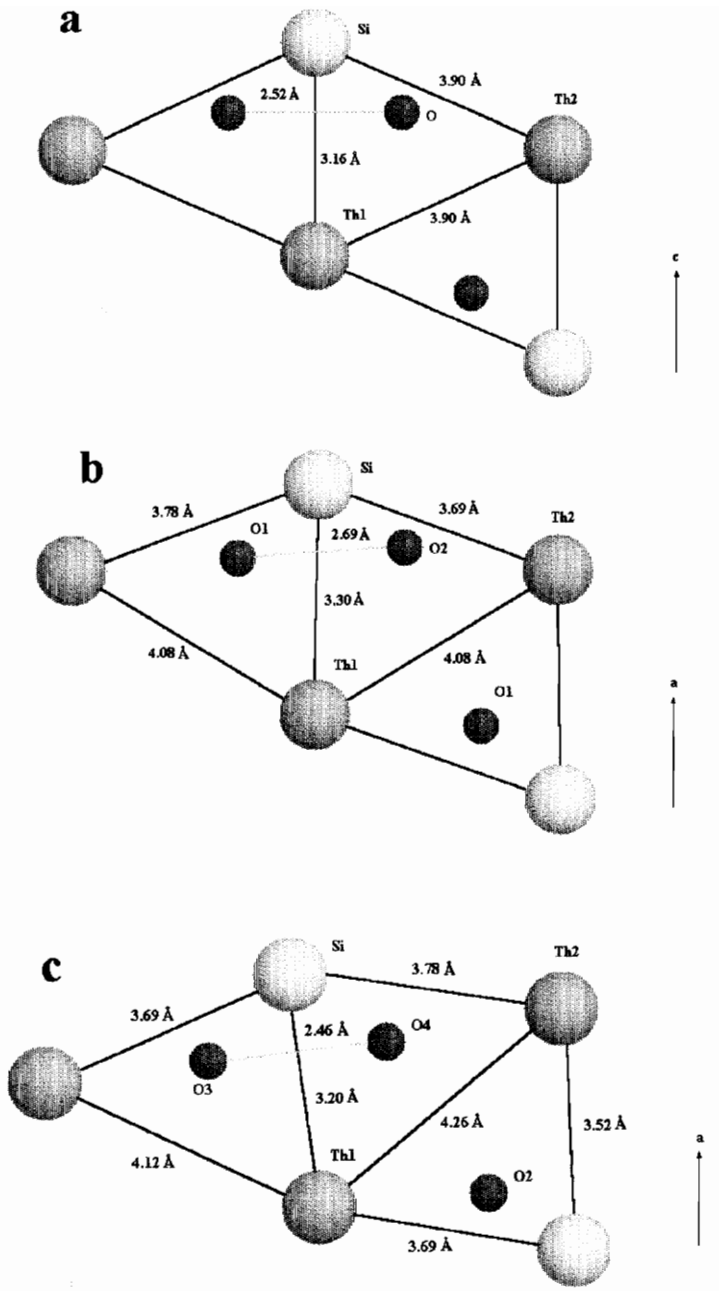

Figure 15. Portions of the structure of thorite $(ThSiO_4)_Z$ and huttonite $(ThSiO_4)_M$. (a) Portion of the (100) of thorite. (b) Portion of the plane parallel to (001) of huttonite. (c) Portion of the (021) of huttonite. Grey lines between oxygens indicate the shared tetrahedral-doddecahedral edge.

(i.e., the distance along the polyhedral chain) increases from 3.16 Å in thorite to 3.30 Å and 3.20 Å in huttonite (Fig. 15). With the increase of this distance the shared edges should both be shorter in huttonite. The longer shared edge in huttonite involves the ninth coordinated, overbonded oxygen, possibly accounting for its greater length. The cation coordination about the oxygen in thorite forms an isosceles triangle with the M1···M2 and M2···T distances being equal. In huttonite it does not, because the M1···M2 distances increase from 3.90A in thorite to 4.08A (smallest of 6 M1···M2 distances) (Fig. 15). The increase of the M1···M2 distances is accompanied by a decrease of the distances of M and T cations of adjacent chains (see Fig. 15). This distance decreases from 3.90 Å in thorite to 3.52 Å (smallest of six values) in huttonite. The M cations must move further apart to accommodate their large radii. The increase in the M···M distances is taken up by moving the M cations closer to the smaller T cations.

The Monazite ⇒ Scheelite Transformation

The monazite ⇒ scheelite transformation is another rarely observed transformation that takes place in compounds such as $LaVO_4$, $PrAsO_4$, $NdAsO_4$, (Stubican and Roy, 1963) and $BiAsO_4$ (Bedlivy and Mereiter, 1982). This transformation is similar in many ways to the zircon ⇒ scheelite transformation, which is not surprising given the similarities between monazite and zircon. Like zircon ⇒ scheelite, pressure is the driving force for the monazite ⇒ scheelite transformation. Stubican and Roy (1963) found the univarient P-T curve for $NdAsO_4$ to be negative, indicating that the transformation monazite to scheelite can proceed by both temperature and pressure paths (Fig. 16). The plane parallel to (001) and the plane parallel to (010) of monazite are sheared to become the closest packed cation planes of the scheelite form (Fig. 14b, 14c). Atomic movements within the planes are also necessary to attain the scheelite packing. The transformation is reconstructive in nature as evidenced by the fact that the transformed product is metastable (Bedlivy and Mereiter, 1982) and that the monazite

Figure 16. P-T phase diagram of the $NdAsO_4$ polymorphs.

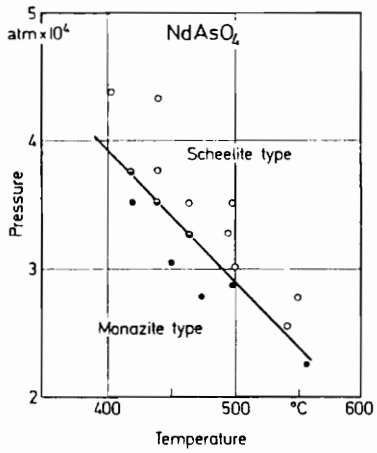

structure has tetrahedra sharing edges with nine-coordinated polyhedra while scheelite has tetrahedra sharing corners with adjacent dodecahedra.

$(Pb_{.5}Th_{.5})VO_4$ has polymorphs in both the scheelite and monazite structures, as well as the zircon structure. $(Pb_{.5}Th_{.5})VO_4$ crystallizes with the scheelite structure at STP. At a temperature of 600°C it undergoes a reconstructive phase transformation to a zircon-type structure. At a temperature of 920°C it undergoes another reconstructive phase transformation to a monazite-type structure (Calestani and Andreetti, 1984). Although a monazite $\Rightarrow$ scheelite transformation does not directly occur in these polymorphs we may still compare the monazite and scheelite forms.

There is a large volume difference between the structures; the monazite form has a volume of 337.29 $Å^3$ and the closest-packed scheelite form has a volume of 319.84 $Å^3$ (a decrease of ~5%). The volume of the M cation polyhedron decreases from 34.20 $Å^3$ in the monazite form to 28.26 $Å^3$ in the scheelite form (a change of ~17%). If the ninth oxygen of the monazite form is excluded, the volume of the MO_8 polyhedron is 28.17 $Å^3$. The volume of the tetrahedron changes little from 2.51 $Å^3$ in the monazite form to 2.59 $Å^3$ in the more dense scheelite form. The tetrahedral quadratic elongation drops from 1.016 to 1.0037. This is easily explained by looking at the (Pb,Th)···V distances along the polyhedral

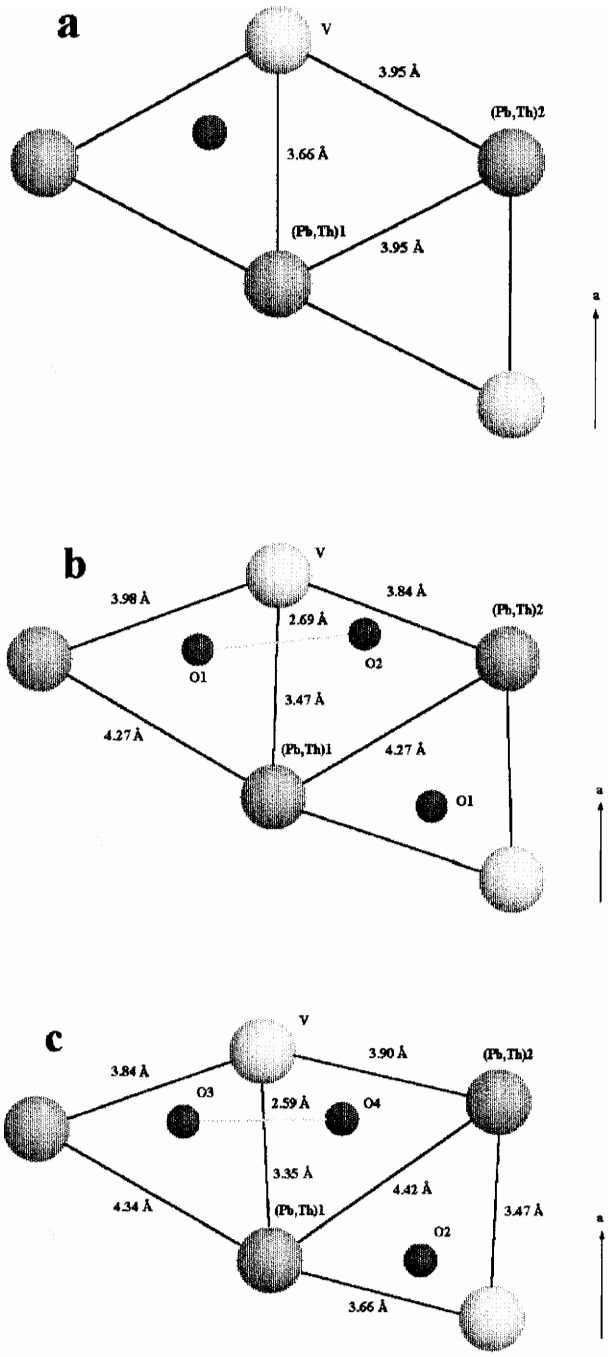

Figure 17. Portions of the the structure of $(Pb_{.5}Th_{.5}VO_4)_S$ and $(Pb_{.5}Th_{.5}VO_4)_M$. (a) Portion of the (112) of $(Pb_{.5}Th_{.5}VO_4)_S$. (b) Portion of the plane parallel to (001) of $(Pb_{.5}Th_{.5}VO_4)_M$. (c) Portion of the (021) of $(Pb_{.5}Th_{.5}VO_4)_M$.

chains (Fig. 17). In the monazite form the distances are 3.47 Å and 3.34 Å, while in the scheelite modification M···T = 3.66 Å. The closer cation-cation distances of the monazite polymorph cause a greater repulsion than in the scheelite polymorph resulting in a more distorted TO_4 tetrahedron.

STRUCTURAL RESPONSE TO CHEMICAL VARIATION AND STRUCTURAL STABILITY FIELDS

The Zircon Structure

Compounds that crystallize with the zircon structure include the trivalent lanthanide (including Sc and Y) vanadates, chromates, arsenates, and phosphates, as well as the tetravalent actinide silicates and tantalum borate (Muller and Roy, 1974) (see Table 2). These compounds are plotted on a graph of rM vs. rT (where rM is the radius of the M cation and rT is the radius of the T cation) cation (Fig. 18). The values for rT rangefrom 0.11 Å (B) to 0.355 Å (V) (Shannon, 1976) rM ranges from 0.74 Å (Ta) to 1.143 Å (Ce). As can be seen from the graph, increasing the size of the M cation eventually causes a transition to the monazite structure. Similarly, increasing the size of the T cation eventually results in a transformation to the scheelite structure. It seems that the zircon structure cannot have a shared tetrahedral edge length greater than ~2.63 Å ($CeVO_4$). Even the zircon-type structure β-$ThGeO_4$ has a shared edge length of 2.61 Å, smaller than that of $CeVO_4$ despite the fact that the radius of Ge exceeds the radius of V by 0.035 Å.

Another trend is also noticeable: as the size of the T cation is increased, the structure is able to accept larger M cations. In the phosphates (rP = 0.17 Å) the cation with the largest rM is terbium at 1.04 Å. In the arsenates (rAs = 0.335 Å) the largest M cation is promethium (rPm = 1.126 Å). The tetrahedron shares two opposite edges with adjacent dodecahedra, therefore an increase in rT will cause an increase in the size of the dodecahedral polyhedra by increasing the length of the shared edge. For example, the

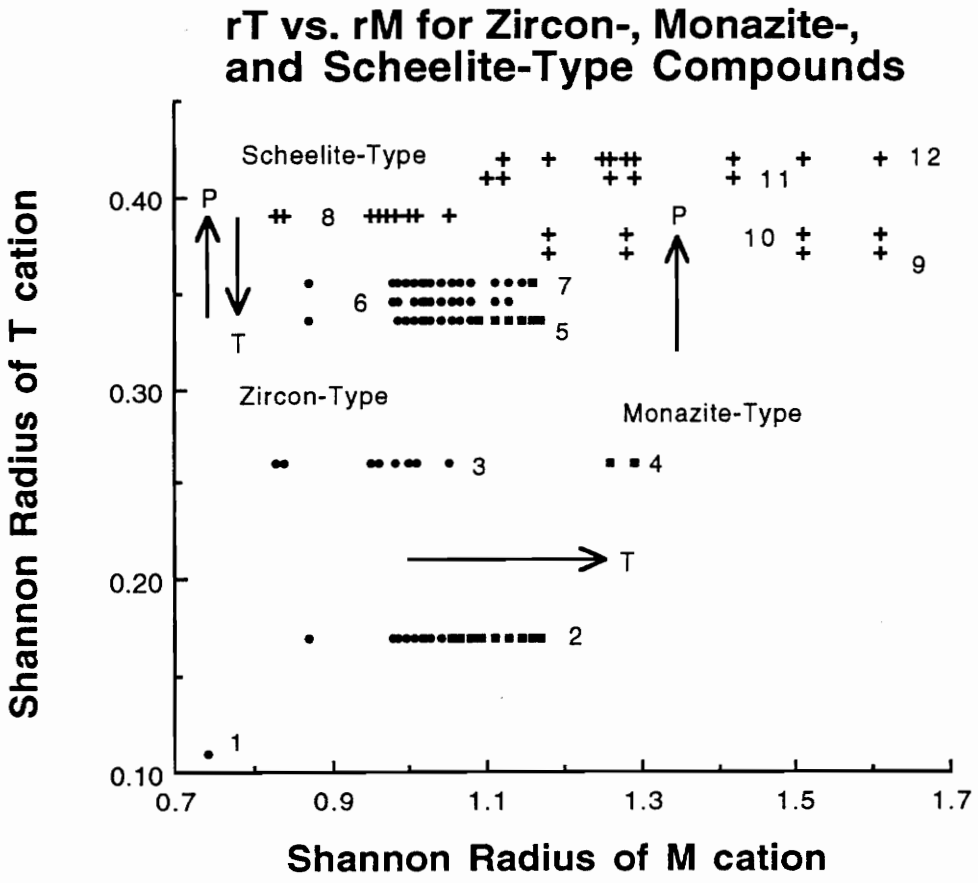

Figure 18. rT vs. rM plot for compounds with the zircon-, monazite-, and scheelite-type structures. Arrows indicate pressure or temperature transformations between structure types. Numbers indicate chemical groups: 1. $TaBO_4$, 2. lanthanide phosphates, 3. actinide silicates, 4. Pb and Sr chromates, 5. lanthanide arsenates, 6. lanthanide chromates, 7. lanthanide vanadates, 8. actinide germanates, 9. alkali technates, 10. alkali rhenates, 11. alkali earth molybdates, and 12. alkali earth tungstates and alkali iodates.

Table 2. Compounds with a zircon-type structure.

Compound	rM, Å	rT, Å	a, Å	c, Å	Vol, Å^3
$ScPo_4$	0.870	0.170	6.5759	5.7949	250.58
YPO_4	1.019	0.170	6.884	6.0202	285.29
$TbPO_4$	1.040	0.170	6.9437	6.0743	292.87
$DyPO_4$	1.027	0.170	6.915	6.0488	289.24
$HoPO_4$	1.015	0.170	6.8884	6.0281	286.03
$ErPO_4$	1.004	0.170	6.8633	6.0087	283.04
$TmPO_4$	0.994	0.170	6.8424	5.9895	280.42
$YbPO_4$	0.985	0.170	6.8169	5.9715	277.50
$LuPO_4$	0.977	0.170	6.7937	5.9582	275.00
$ScVO_4$	0.870	0.355	6.7803	6.1349	282.04
YVO_4	1.019	0.355	7.1193	6.2892	318.76
$CeVO_4$	1.143	0.355	7.4013	6.498	355.96
$PrVO_4$	1.126	0.355	7.364	6.4654	350.61
$NdVO_4$	1.109	0.355	7.3315	6.4359	345.94
$SmVO_4$	1.079	0.355	7.2654	6.3876	337.18
$EuVO_4$	1.066	0.355	7.2373	6.3661	333.45
$GdVO_4$	1.053	0.355	7.2131	6.3491	330.34
$TbVO_4$	1.040	0.355	7.177	6.3263	325.86
$DyVO_4$	1.027	0.355	7.148	6.3067	322.23
$HoVO_4$	1.015	0.355	7.1237	6.289	319.15
$ErVO_4$	1.004	0.355	7.0973	6.2721	315.94
$TmVO_4$	0.994	0.355	7.0693	6.2584	312.76
$YbVO_4$	0.985	0.355	7.0439	6.247	309.95
$LuVO_4$	0.977	0.355	7.0263	6.2329	307.71
$AmVO_4$	1.090	0.355	7.31	6.42	343.06
$PmVO_4$	1.093	0.355	7.266	6.394	337.57
$PrCrO_4$	1.126	0.345	7.344	6.428	346.69
$NdCrO_4$	1.109	0.345	7.311	6.402	342.19
$EuCrO_4$	1.066	0.345	7.223	6.33	330.25
$GdCrO_4$	1.053	0.345	7.204	6.315	327.73
$SmCrO_4$	1.079	0.345	7.251	6.356	334.18
$TbCrO_4$	1.040	0.345	7.17	6.294	323.57
$DyCrO_4$	1.027	0.345	7.143	6.274	320.11
$HoCrO_4$	1.015	0.345	7.12	6.255	317.09
$YCrO_4$	1.019	0.345	7.112	6.251	316.18
$ErCrO_4$	1.004	0.345	7.093	6.239	313.89
$YbCrO_4$	0.985	0.345	7.058	6.216	309.65
$TmCrO_4$	0.994	0.345	7.066	6.22	310.55

Table 2, continued

Compound	rM, Å	rT, Å	a, Å	c, Å	Vol, Å^3
$PmCrO_4$	1.093	0.345	7.28	6.38	338.13
$LuCrO_4$	0.977	0.345	7.027	6.2	306.15
$CaCrO_4$	1.120	0.260	7.2327	6.2806	328.55
$GdAsO_4$	1.053	0.335	7.14	6.34	323.21
$SmAsO_4$	1.079	0.335	7.2	6.4	331.78
$DyAsO_4$	1.027	0.335	7.09	6.315	317.44
$YAsO_4$	1.019	0.335	7.06	6.3	314.01
$YbAsO_4$	0.985	0.335	6.99	6.24	304.89
$EuAsO_4$	1.066	0.335	7.1541	6.3953	327.32
$ErAsO_4$	1.004	0.335	7.045	6.3	312.68
LuAsO	0.977	0.335	6.952	6.23	301.10
PmAsO	1.097	0.335	7.31	6.43	343.59
$TbAsO_4$	1.040	0.335	7.1025	6.3536	320.51
$TmAsO_4$	0.994	0.335	6.9939	6.2595	306.18
$HoAsO_4$	1.015	0.335	7.0548	6.3159	314.34
$ScAsO_4$	0.870	0.335	6.7101	6.1126	275.22
$ZrSiO_4$	0.840	0.260	6.6042	5.9796	260.80
$HfSiO_4$	0.830	0.260	6.5725	5.9632	257.60
$USiO_4$	1.000	0.260	6.981	6.25	304.59
$ThSiO_4$	1.050	0.260	7.128	6.314	320.80
$PaSiO_4$	1.010	0.260	7.068	6.288	314.13
$NpSiO_4$	0.980	0.260	6.95	6.243	301.55
$PuSiO_4$	0.960	0.260	6.906	6.221	296.70
$AmSiO_4$	0.950	0.260	6.87	6.2	292.62
$TaBO_4$	0.740	0.110	6.214	5.486	211.84

shared edge length in $TbPO_4$ (rTb = 1.04 Å, rP = 0.17 Å) is 2.41 Å but it is 2.57 Å in $TbAsO_4$ (rAs = 0.335 Å) and 2.63 Å in $TbVO_4$ (rV = 0.355 Å). The dodecahedral volumes are 23.74 Å^3, 24.25 Å^3, and 24.47 Å^3 respectively, inspite the fact that the M cation is the same in all three compounds (Fig. 19).

As Carron et. al. (1958) have pointed out, one may use rM to T-O bond length ratio to predict the structure of rare earth phosphates, vanadates, and arsenates. By computing this ratio for compounds that fall on or near the structural border between zircon and monazite (see Fig. 18) we may estimate a ratio *r* (*r* = 1:1.56) such that values

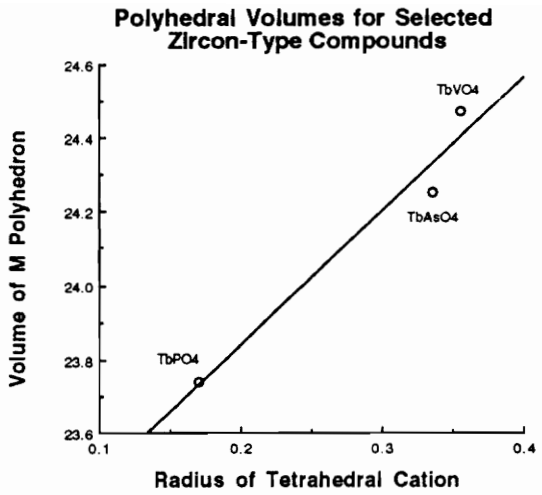

Figure 19. Plot of the M polyhedral volumes of $TbPO_4$, $TbAsO_4$, and $TbVO_4$ vs. rT.

$<r$ have the monazite structure and values $>r$ have the zircon structure. This r value works well except in one case (see Table 3). Chromatite ($CaCrO_4$) crystallizes in the zircon structure but has an r ratio of 1:1.54, suggesting that it should have the monazite structure.

Table 3. *r* ratios for zircon-type compounds near the zircon/monazite structural border.

Compound	rM, Å	T-O, Å	*r*
$TbPO_4$	1.040	1.55	1.49
$ThSiO_4$	1.050	1.64	1.56
$PmAsO_4$	1.093	1.71	1.56
$PrCrO_4$	1.126	1.72	1.53
$CeVO_4$	1.143	1.73	1.52

Multiple regressions were performed for the primary structural parameters of the zircon structure. These parameters included unit cell edge lengths, unit cell volume, oxygen positional parameters, M-O bond lengths (2 unique), the T-O bond length, polyhedral volumes, O-T-O bond angles, tetrahedral quadratic elongations, and the T-O-M1, T-O-M2, and M-O-M angles. The data for these regressions are taken from 27

structure refinements (see Appendix A). The bond angles, bond lengths, etc. were calculated using the program Metric 3.0 (Boisen et al, 1993). The regression equations were calculated with the statistical program JMP (equation form is given in Table 4). The results are summarized in Table 4 and discussed below.

Table 4. Coefficients of regression equations of zircon-type compounds.

Equations are of the form: A(rM) + B(rT) + C(q x q) + D

Parameter	A	B	C	D	R^2	Fig.
T vol, Å^3	0.2209	3.5646	0.0000	1.0194	0.997	A2
T-O, Å	0.0274	0.9201	0.0054	1.2724	0.997	A1
TQE	-0.0088	0.0323	0.0126	0.8209	0.986	A15
M1-O, Å	1.1210	-0.0279	0.0245	0.8004	0.996	A3
M2-O, Å	0.7098	0.3406	0.0000	1.5948	0.983	A4
M vol, Å^3	26.3448	4.7845	0.0000	-4.5783	0.994	A9
O-T-O, °	3.7580	-13.6071	-3.9954	161.2640	0.976	A12
T-O-M1,°	5.4612	-15.4438	-2.8826	195.3989	0.976	A10
T-O-M2, °	6.3733	-4.7871	2.5271	54.5898	0.939	A9
M-O-M, °	-12.6622	20.3019	0.0000	116.1756	0.981	A11
a, Å	2.2442	1.2208	0.0111	4.2424	0.995	A6
c, Å	1.5530	1.4284	0.1316	2.2262	0.991	A7
Volume, Å^3	268.9431	169.5629	7.9269	-133.4857	0.993	A8
y	0.0504	-0.0521	0.0043	-0.0321	0.983	A13
z	0.0432	-0.0769	-0.0058	0.2718	0.988	A14

The parameters of the zircon structures were at first refined as a function of the Shannon (1976) radii of the cations, rM and rT. In several cases this proved unsatisfactory (T-O-T angles, c cell edge, T volume). Because the cation repulsions are very high in compounds with the zircon structure, it stands to reason that this repulsion has a significant effect on the structure (an effect noted for the ordered clinopyroxenes by Ribbe and Prunier, 1977). In this study, q is defined as the product of the M and T cation charges. It proved to be effective in accounting for the cation repulsions and their effect on various stereochemical, atomic, and structural parameters.

Tetrahedral distortions show interesting variations in compounds with the zircon structure (see Fig. A15). The tetrahedral distortions decrease with increasing rM. This may be explained by non-bonded interaction between cations. The spacing between cations along the polyhedral chains in the structure is close, giving rise to high tetrahedral quadratic elongations in some compounds. The cations repel each other, resulting in elongation of the tetrahedra along (001). When larger M cations are substituted for smaller ones the cation-cation distance along the chain increases. With the cations further apart the electrostatic repulsion between them is less and thus the tetrahedral strain decreases.

The change in tetrahedral quadratic elongation with increasing T cation size is just the opposite, larger T cations have more distorted tetrahedra. This may be explained in the following manner. Increasing the size of the T cation will increase the length of the tetrahedral edges. However, the shared edges do not lengthen as much as the unshared edges due to the strong cation-cation repulsions across the edge. This can be seen by looking at the shared and unshared tetrahedral edge lengths in $TbPO_4$, $ThSiO_4$, $TbAsO_4$, and $TbVO_4$ plotted on Figure 20. Thus increasing the size of the T cation will distort the tetrahedra despite the fact that the cations are farther apart and the electrostatic repulsion is slightly less.

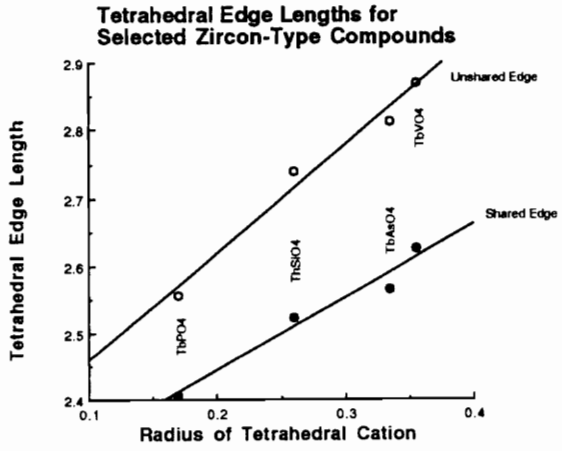

Figure 20. Plot of shared and unshared tetrahedral edge lengths vs. rT for $TbPO_4$, $ThSiO_4$, $TbAsO_4$, and $TbVO_4$.

The polyhedral volumes and cation-oxygen distances were modeled successfully with high correlation coefficients. The volume of the M cation polyhedra (Fig. A5) showed a marked dependence of the radius of the tetrahedral cation as well as the radius of the M cation as seen in the F-ratios: rT = 109 and rM = 2793 (The F-ratio indicates the degree to which the variable affects the regression equation, larger F-ratio = greater effect). This supports the earlier conclusion that the size of the T cation affects the size of the dodecahedra due to the shared tetrahedral-dodecahedral edge. The M-O1 distances (Fig. A3) showed a slight dependence on q. This distance is the short M-O distance and represents a bond to an oxygen of the shared tetrahedral-dodecahedral edge. Because the M-T distances are close across the shared edge, it is no surprise that the charges of the cations have an effect on the M-O1 distance.

The bond angles modeled well but less well than the bond distances and volumes. The T-O-M2 angle (Fig. A9) showed a strong dependence on rT (F = 441) as well as q (F = 105). The T-O-M1 angle (Fig. A10) showed almost the opposite trend with the an rT F-ratio of 107 and a q-term F-ratio of 204. The O-T-O angles (Fig. A12) also showed a strong dependence on q while the M-O-M angle (Fig. A11) showed no dependence on q at all. Once again, the parameters most strongly related to the shared tetrahedral-dodecahedral edge show a strong dependence on q.

Regressions of the unit cell parameters showed very high correlation coefficients (0.995 and above). The unit cell volumes, a, and c cell edge lengths were modeled with the data in Table 2. The arsenates showed marked deviations in the a and c cell edge plots (Fig. A6 and A7). Therefore, the arsenate data were excluded from the regressions of a and c but are plotted on the regression graphs. The c cell edge length (Fig. A7) showed nearly equal dependence on rT and rM (F-ratios for rT = 1062, rM = 1391) and a significant dependence on q (F-ratio of 254). The c direction is of course the direction in which the closest M···T distances are found. The oxygen positional parameters (Fig. A13 and A14) showed strong correlation coefficients: y = 0.983 and z = 0.987. Both parameters displayed a greater dependence on rT than on rM or q.

Several compounds yielded data that were "consistently inconsistent" with the other data. Both $ThSiO_4$ (thorite) and β-$ThGeO_4$ produced such data. The structure refinements for these compounds were computed from x-ray diffraction data (Taylor and Ewing, 1978, and Ennaciri et. al., 1986). Thorium in these compounds has many more electrons (Z = 90) than the other atoms, so it scatters most of the x-rays, thus the very light oxygens (Z = 8) are virtually invisible. Therefore it is difficult to accurately refine the oxygen positional parameters. α-$(ThGeO_4)_S$ and huttonite $(ThSiO_4)_M$ showed similar deviations in the scheelite and monazite regressions, respectively. The three lanthanide arsenates studied ($DyAsO_4$, $LuAsO_4$, and $TbAsO_4$) also showed rather large, unexplained deviations from the other compounds. Data for these compounds were not used in the regressions, but they were plotted on the regression graphs to indicate the degree of their variations.

The Scheelite Structure

The scheelite structure is adopted by molybdates and tungstates with the following bivalent M cations: Ca, Ba, Sr, Cd, Pb, and Er; germanates with tetravalent actinide M cations: Th, U, Pa, Pu, Np, Zr, and Hf; and technates, rhenates and iodates with monovalent M cations such as: Ag, Na, K, and Rb (Muller and Roy, 1974) (Table 5). These compounds are plotted along with zircon- and monazite-type on Figure 23, where it can be seen that the scheelite-type structure accepts a wide range of M cation sizes (from Hf^{4+} = 0.83 Å to Rb^{+} = 1.61 Å) but a rather narrow range of T cation sizes (from Tc^{7+} = 0.37 Å to I^{7+}, W^{6+} = 0.42 Å). The scheelite structure also accepts a variety of charge combinations such as +4,+4 (germanates), +2,+6 (molybdates and tungstates), and +1,+7 (technates, rhenates, and, iodates). Linear regressions were performed to model the major structural parameters of the scheelite structure. The data set consisted of 12 scheelite crystal structure refinements, structural parameters were calculated from the refinements with the program Metric 3.0 (see Appendix B). Results of the regressions

Table 5. Compounds with the scheelite-type structure.

Name	rM, Å	rT, Å	a, Å	c, Å	Vol, Å^3
$AmGeO_4$	0.95	0.39	5.033	11.05	279.91
$PuGeO_4$	0.96	0.39	5.04	11.11	282.21
$NpGeO_4$	0.98	0.39	5.061	11.16	285.85
$UGeO_4$	1.00	0.39	5.084	11.226	290.16
$CeGeO_4$	0.97	0.39	5.0396	11.1551	283.31
$HfGeO_4$	0.83	0.39	4.8546	10.4945	247.32
$ThGeO_4$	1.05	0.39	5.1397	11.5406	304.86
$ZrGeO_4$	0.84	0.39	4.8754	10.5585	250.97
$PaGeO_4$	1.01	0.39	5.106	11.38	296.69
$NaReO_4$	1.18	0.38	5.362	11.718	336.91
$AgReO_4$	1.28	0.38	5.349	11.916	340.94
$KReO_4$	1.51	0.38	5.615	12.5	394.10
$RbReO_4$	1.61	0.38	5.803	13.167	443.40
$KTcO_4$	1.51	0.37	5.654	13.03	416.54
$RbTcO_4$	1.61	0.37	5.758	13.54	448.91
$NaTcO_4$	1.18	0.37	5.337	11.88	338.38
$AgTcO_4$	1.28	0.37	5.317	11.87	335.57
$AgIO_4$	1.28	0.42	5.368	12.013	346.16
KIO_4	1.51	0.42	5.75	12.63	417.58
$NaIO_4$	1.18	0.42	5.3354	11.9454	340.04
$RbIO_4$	1.61	0.42	5.874	12.938	446.41
$CaWO_4$	1.12	0.42	5.4312	12.1065	357.12
$SrWO_4$	1.26	0.42	5.1539	11.192	297.29
$BaWO_4$	1.42	0.42	5.2256	11.434	312.23
$PbWO_4$	1.29	0.42	5.3936	12.019	349.64
$EuWO_4$	1.25	0.42	5.5804	12.818	399.16
$PbMoO_4$	1.29	0.41	5.2419	11.376	312.58
$CdMoO_4$	1.10	0.41	5.4136	11.942	349.98
$CaMoO_4$	1.12	0.41	5.6148	12.721	401.04
$SrMoO_4$	1.26	0.41	5.4355	12.108	357.73
$BaMoO_4$	1.42	0.41	5.4151	11.942	350.18

are summarized in Table 6 and discussed below. Structural parameters were modeled as a function of rM and rT as well as q (see Table 6 for form of the equation). The q term only yielded significant F-ratios when used as a second-order polynomial.

Table 6. Coefficients of regression equations of scheelite-type compounds.

Equation are of the form: A(rM) + B(rT) + C1(q^2) + C2(q) + D

Parameter	A	B	C1	C2	D	R^2	Fig.
T vol, Å^3	0.0	5.1355	-0.0001	0.0126	0.6005	0.975	B2
T-O, Å	0.0	1.1874	0.0005	-0.0089	1.3085	0.973	B1
M1-O, Å	0.9720	0.0	0.0	0.0	1.3474	0.991	B3
M2-O, Å	0.9652	0.8979	0.0034	-0.0762	1.4387	0.999	B4
M vol, Å^3	33.6083	0.0	0.0630	-1.3833	-3.6006	0.998	B5
O-T-O, °	3.2432	-11.5459	-0.0763	1.4573	101.8806	0.994	B12
T-O-M1, °	20.5720	-61.3685	-0.1086	2.3205	122.3796	0.995	B9
T-O-M2, °	-2.5625	24.9156	0.0885	-1.8849	122.7300	0.945	B10
M-O-M, °	-11.4112	18.3587	0.0601	-1.0310	112.6337	0.998	B11
a, Å	1.2089	1.533	0.0	0.0	3.2506	0.998	B6
c, Å	3.4592	0.0	0.0	0.0	7.6412	0.981	B7
volume, Å^3	271.6250	350.1570	0.7590	-15.5200	-59.2944	0.998	B8
x	-0.0333	0.0	-0.0003	0.0043	0.2893	0.994	B13
y	-0.0850	0.1790	0.0	0.0	0.1718	0.979	B14
z	-0.0336	0.6263	0.0	0.0	-0.1372	0.940	B15

The tetrahedral quadratic elongation showed significant non-linear behavior when modeled as a function of rM (see Fig. 21). The tetrahedral cation radius and q contributed only very slightly to regressions of quadratic elongation (second order fit with rM yields a corellation coefficient of 0.976). The distribution of data in this plot strongly resembles plots of the electrostatic repulsive force vs. distance between two oppositely charged point masses. A possible interpretation may come from the packing of the cations. The highly charged cations of these compounds are in a closest packed array. At such short distances it is likely that electrostatic forces are dominant in determining atomic positions. Because the positions of the cations are fixed by symmetry it is the anions that respond to the electrostatic repulsions, and the positions of the anions determine the shapes of the coordinated polyhedra.

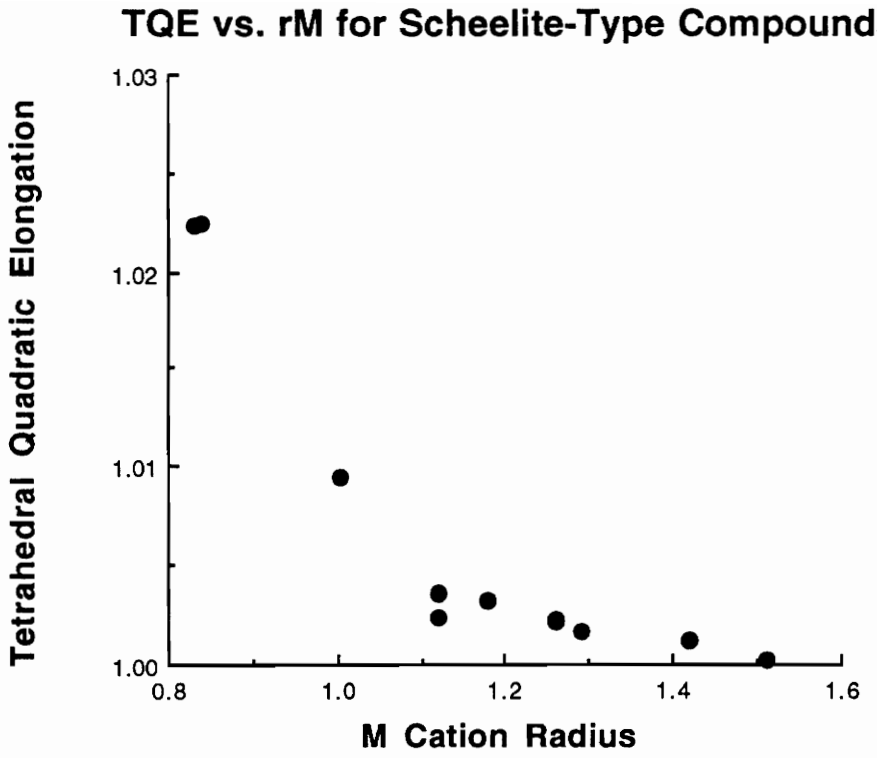

Figure 21. Plot of TQE vs. rM for scheelite-type compounds.

The cation-oxygen distances and polyhedral volumes were modeled with reasonable success. The T-O distance and the tetrahedral volume (Fig. B1 and B2), as functions of rT and q, yielded correlation coefficients of 0.97. The M-O distances and MO_8 volume yielded much better correlation coefficients. The M-O1 distance (Fig. B3) required only the M radius to yield a correlation coefficient of 0.99. The M-O2 distance (Fig. B4) required the addition of both rT and q to yield a fit of 0.999. The M polyhedral volume (Fig. B5) also required all three variables to yield a fit of 0.997.

All of the bond angles modeled required q for a high correlation coefficient. The O-T-O angles (Fig. B12) fit well when all three parameters were used in the regression. The M radius and q had almost identical F-ratios (40 and 38 respectively), both of which were greater than the rT F-ratio (11). T-O-M1 (Fig. B9) was a function of rM over the

other variables. The T-O-M2 angle (Fig. B10) was a function of q and rT more than rM (F-ratios 11, 10 , and 5 respectively). The M-O-M angle (Fig. B11) depended on rM significantly more than q or rT (F-ratios of 280, 25, and 16 respectively). The correlation coefficients for T-O-M1, T-O-M2 and M-O-M were 0.995, 0.945, and 0.997 respectively.

Unit cell parameters modeled well. The unit cell volume and a and c cell edge lengths (Fig. B6, B7, and B8) were influenced by rM much more than the other variables. Correlation coefficients exceeded 0.99 for all but the c cell edge. The oxygen positional parameters showed a great variation in fit and variable dependence. The x coordinate (Fig. B13) fit well (0.993) as a function of rM and q. The F-ratio of q (41) was almost exactly half that of rM F-ratio (85). The y positional parameter (Fig. B14) fit less well (correlation coefficient = 0.979) as a function of the radii of the cations. The rM was much more significant to the regression than rT. The z coordinate (Fig. B15) was fit as a function of the cation radii. The F factor for rT (102) was much larger than that of rM (31). It should be noted that the regression plot for z shows two significant groupings of points (i.e. in essence the regression line ran though two points).

α-$ThGeO_4$ showed slight to large deviations in all regression equations. It is surmised that structure refinements of this compound suffer from the same sort of difficulties obtained with thorite discussed earlier. α-$ThGeO_4$ was therefore excluded from the regression equations. The α-$ThGeO_4$ data have been included in the regression plots to demonstrate their inconsistencies.

The Monazite Structure

Compounds with the monazite structure include: the lanthanide phosphates from Gd^{3+} to La^{3+}, arsenates from Nd^{3+} to La^{3+}, chromates from Pr^{3+} to La^{3+}, and $LaVO_4$ as well as PbCrO4 (crocoite), $SrCrO_4$, $PbSeO_4$, $SrSeO_4$, and $ThSiO_4$ (huttonite) (Muller and Roy, 1974) (Table 7). This structure accomodates the same size range for T cations

Table 7. Compounds with the monazite-type structure.

Compound	rM, Å	rT, Å	a, Å	b, Å	c, Å	β, °	Vol, Å^3
$LaPO_4$	1.160	0.170	6.8402	7.0805	6.5064	103.34	306.62
$CePO_4$	1.143	0.170	6.7984	7.0234	6.4731	103.44	300.61
$PrPO_4$	1.126	0.170	6.7754	6.9879	6.4452	103.59	296.61
$NdPO_4$	1.109	0.170	6.7433	6.959	6.4101	103.66	292.29
$PmPO_4$	1.093	0.170	6.72	6.89	6.37	104.28	285.8
$SmPO_4$	1.079	0.170	6.6878	6.8943	6.3712	103.89	285.17
$EuPO_4$	1.066	0.170	6.6682	6.8654	6.3539	103.94	282.32
$GdPO_4$	1.053	0.170	6.6546	6.8486	6.3372	104.02	280.21
$AmPO_4$	1.090	0.170	6.73	6.93	6.41	103.83	290.68
$BiPO_4$	1.170	0.170	6.752	6.933	6.468	103.72	294.12
$LaAsO_4$	1.160	0.335	7.008	7.212	6.767	104.48	331.12
$CeAsO_4$	1.143	0.335	6.957	7.158	6.738	104.72	324.56
$PrAsO_4$	1.126	0.335	6.929	7.119	6.715	104.8	320.26
$NdAsO_4$	1.109	0.335	6.897	7.094	6.685	104.9	316.08
$AmAsO_4$	1.090	0.335	6.89	7.06	6.62	105.5	310.28
$LaVO_4$	1.170	0.335	7.0451	7.284	6.7232	104.86	333.47
$PbCrO_4$	1.290	0.260	7.127	7.438	6.799	102.43	351.14
$SrCrO_4$	1.260	0.260	7.065	7.375	6.741	103.08	344.57
$SrSeO_4$	1.260	0.280	7.101	7.3400	6.874	103.48	342.10
$PbSeO_4$	1.290	0.280	7.154	7.407	6.954	103.14	358.80
ThSiO4	1.050	0.260	6.784	6.974	6.5	104.92	297.14

(P^{+5} = 0.17 Å to V^{+5} = 0.355 Å) as the zircon structure but a more restricted size range for the M cation (Pb^{+2} = 1.19 Å to Gd^{+3} = 1.053 Å). The monazite structure accepts the same charge combinations as the zircon structure (+4,+4; +3,+5) with the addition of +2, +6. Modeling of the structural parameters of the monazite structure has been attempted using 12 structure refinements; structural parameters were obtained from Metric 3.0. The structural parameters are summarized in Appendix C and the regression equations are summarized in Table 8 and discussed below.

Table 8. Coefficients of regression equations for monazite-type compounds.

Equations are of the form: A(rM) + B(rT) + C(q x q) + D

Parameter	A	B	C	D	R^2	Fig.
xM	-0.0318	-0.0468	0.0012	0.2076	0.998	C1
yM	0.0292	-0.0044	0.0006	0.1157	0.560	C2
zM	0.0026	-0.0313	0.0024	0.2474	0.997	C3
xT	0.0228	-0.0367	0.0007	0.6620	0.993	C4
yT	0.0251	0.0055	0.0007	0.1238	0.993	C5
zT	0.0170	-0.0218	0.0007	0.2779	0.988	C6
xO1	0.1083	-0.0814	0.0	0.0862	0.974	C7
yO1	0.0613	-0.0511	0.0011	0.4283	0.974	C8
zO1	-0.0152	-0.0060	-0.0025	0.2704	0.544	C9
xO2	-0.0218	-0.0359	-0.0022	0.1810	0.981	C10
yO2	-0.0336	0.0690	-0.0010	-0.1263	0.992	C11
zO2	0.0211	-0.0344	-0.0005	0.1087	0.955	C12
xO3	0.1075	-0.0765	0.0013	0.5410	0.990	C13
yO3	0.0475	-0.0039	0.0032	0.0034	0.980	C14
zO3	0.0084	0.0412	0.0017	0.4332	0.968	C15
xO4	0.0937	-0.1627	0.0	0.3363	0.972	C16
yO4	0.0326	0.0264	0.0014	0.1528	0.931	C17
zO4	0.0897	-0.0735	0.0029	-0.0060	0.919	C18
a, Å	1.5903	1.2114	0.0072	4.3363	0.999	C23
b, Å	2.1148	1.1620	0.0	4.4087	0.998	C24
c, Å	2.6638	0.6412	0.0	5.0680	0.997	C25
β, °	3.0836	-4.0070	-0.0964	125.0835	0.978	C26
volume, Å^3	243.7955	150.4768	0.0	-3.8880	0.998	C27
TQE	-0.0155	0.0358	-0.0026	1.0552	0.990	C28
M-O, Å	0.9036	0.1000	0.0	1.5072	0.997	C21
T-O, Å	0.0	0.9532	0.0	1.3758	0.999	C19
M vol, Å^3	2.0102	34.8500	0.0	-7.6091	0.996	C22
T vol, Å^3	0.0	3.7367	0.0	1.2184	0.998	C20
M-O-M, °	-21.0384	23.5314	0.0	129.7546	0.997	C31
T-O1-M1, °	23.8730	-22.4720	0.3702	114.2885	0.969	C29
T-O1-M2, °	-10.2723	-1.2198	-0.1556	119.2859	0.890	C30

The regression equations utilized the rM, rT, and q. Regression equations for many of the parameters investigated (atomic positions, interatomic distances and angles, lattice parameters, etc.) evidenced very high correlation coefficients. Several compounds,

however, did not fit well with the others in terms of atomic positions, and one of these compounds was crocoite ($PbCrO_4$). This deviation may be easily explained by the presence of lead. Because lead has one lone-electron pair it tends to form one-sided bonds. This tendency has the effect of changing some bond lengths and positional parameters from what they would be based on spherical cation size considerations alone. Bismuth is another element that forms one sided bonds due to a lone-electron pair. The compound $BiAsO_4$ (rooseveltite) crystallizes with the monazite structure (Bedlivy and Merierter, 1982) and has the same sort of deviation of positional parameters and bond lengths as crocoite. This deviation is especially evident in the Bi-O lengths. The ninth-coordinated oxygen is a distance of 3.24 Å while the next nearest is at a distance of 2.64 Å, a significantly larger difference than in the other monazite compounds. The Bi-O bond length of 3.24 Å is greater than the smallest Bi···As distance of 3.22 Å and should, therefore, be considered non-bonded (Bedlivy and Merierter, 1982). In crocoite the longest Pb-O bond length is 3.08 Å while the next nearest Pb-O bond length is 2.81 Å. The closest Pb···Cr is 3.33 Å indicating the the ninth oxygen should be considered bonded.

Two other compounds also showed deviations: $SrCrO_4$ and $SrSeO_4$. In fact these compounds showed significant deviations in atomic positions from each other. Because the radius of Cr^{6+} (0.26 Å) is almost equal to that of Se^{6+} (0.28 Å) one would expect the compounds to be nearly identical, similar to the silicates, zircon and hafnon (rZr^{4+} = 0.84 Å and Hf^{4+} = 0.83 Å). Refinements of both structures were undertaken by Effenberger and Pertlik (1986), who give no explanations for such variations. Using one of these compounds in the regression equations without the other seemed to yield good fits. In fact it appeared that both worked equally well when used without the other. Because this seems to be the case, $SrCrO_4$ was used in the regressions and not $SrSeO_4$. The last compound to show deviations was huttonite ($ThSiO_4$). Reasons for its deviations hinge on the presence of thorium and have been discussed in the section on zircon structures.

Huttonite, crocoite, and $SrSeO_4$ have been included in plots of the regressions but excluded from the calculation of the regression equations.

Regressions of the eighteen independent atomic positional parameters of the monazite structure yielded surprisingly high correlation coefficients. The fractional coordinates of the M and T cations yielded the best fits. This is not surprising because these atoms have many electrons to scatter x-rays (especially the M cation) and thus scatter x-rays better than the oxygens. The correlation coefficients were in the 0.995 range except for the y coordinate of M (Fig. C2) which yielded a fit with a correlation coefficient of only 0.5. The plot of the z coordinate of M (Fig. C3) showed an extreme clustering of data, so that the regression line was essentially drawn through three points. The oxygen positional parameters all showed smaller correlation coefficients (mean 0.95) but still fit well overall. Because there are so many coordinates they are not discussed individually but the reader is refereed to Table 8 and Appendix C for a full display of the results.

Fits of bond lengths and polyhedral volumes for monazite type-compounds yielded correlation coefficients of 0.998 and above. The plots for the average T-O bond length (Fig. C19) and the tetrahedral volume (Fig. C20) show extreme clustering of data points, indicating very little variation of the tetrahedron with M cation substitutions (this is also borne out by the fact that T-O was fit only to rT with a correlation coefficient of 0.999). The q term played little role in any of these regressions.

The tetrahedral quadratic elongation (Fig. C28) modeled well with a fit of 0.990 as a function of rM, rT, and q. The rM seems to play little role in quadratic elongation with an F-ratio of 13. The rT and q both proved to be significant with F-ratios of 291 and 121 respectively. Like the zircon structure, q significantly improves the regression of the tetrahedral quadratic elongation.

The bond angles (Fig. C29, C30, and C31) of the monazite compounds modeled less well than other parameters. The q-term seemed not to play a significant role in the regressions. The M1-O1-M2 and T-O1-M1 angles were more influenced by rT than rM.

The T-O1-M2 angle proved to be more a function of rM. These bond angles fit with correlation coefficients of 0.997, 0.969 and 0.890 respectively.

Regressions of cell edges and unit cell volume yielded good fits. The a cell edge length (Fig. C23) proved to be more dependent on rT than rM while the b and c cell edge lengths (Fig. C24 and C25) were more dependent on rM. The q term proved to be of little consequence to the cell edge lengths. The a, b , and c cell edges yielded correlation coefficients in the 0.997 range. The angle β (Fig. C26) proved to be significantly dependent on rT. β fit with a correlation coefficient of 0.978. The unit cell volume regression (Fig. C27) yielded a correlation coefficient of 0.998.

Conclusions

The structures of zircon, monazite, and scheelite are very closely related. Similar structural elements occur in each: alternating polyhedral chains and planes of closest packed or pseudo-closest packed cations. Using these features one may place the unit cells of these compounds may analogously orientated. Once this is accomplished the geometrical aspects of the reconstructive phase transformations becomes evident. These phase transformations involve changing the cation planes of one structure-type to the cation planes of another. Phase transformations may also occur as a function of composition as a plot of rM vs. rT of compounds with the zircon, scheelite, and monazite structure-types clearly showed (Fig. 18). Regression equations for crystal structure parameters (bond lengths, bond angles, polyhedral volumes, unit cell edge lengths and tetrahedral quadratic elongation) as a function of composition (rM, rT, and q) clearly show systematic variations.

References

Aldred, A. T. (1984) Crystal chemistry of ABO_4 compounds. American Chemical Society Symposium Serial Number 246. Geochemical Behavior of Disposed Radioactive Wastes, edited by G. S. Barney, J. D. Navratil, and W. W. Schultz, pp. 305-314. Washington D. C.: American Chemical Society.

Bayer, G. (1978) Zur Kristallchemie des Zirkons und des Scheelits. Schweizerische Mineralogische und Petrographesche Mittielungen, 58, 111-126.

Bedlivy, D. and Mereiter, K. (1982) Structure of α-$BiAsO_4$ (Rooseveltite). Acta Crystallographica, B38, 1559-1561.

Binks, W., (1926) The crystalline state of zircon. Mineralogy Magazine, 21, 176.

Brown, R. J. C., Powell, B. M., and Stuart, S. N. (1993) Thermal effects in the structure of potassium perrhenate. Acta Crystalographica, C49, 214-216.

Calestani, G. and Andreetti, D. (1984) The crystal structure of the $Pb_{.5}Th_{.5}VO_4$ polymorphs with the scheelite, zircon, and huttonite-type structures. Zeitscrift für Kristallographie, 168, 41-51.

Carron, M. K., Mrose, M. E., and Murata, K. J. (1958) Relation of the ionic radius to the structures of rare-earth phosphates, arsenates, and vanadates. American Mineralogist, 43, 985-989.

Chakoumakos, B. C., Abraham, M. M., and Boatner, L. A. (1994) Crystal structure refinements of the zircon-type MVO_4 (M = Sc, Y, Ce, Pr, Nd, Tb, Ho, Er, Tm, Yb, Lu). Journal of Solid State Chemistry, 109, 197-202.

Effenberger, H., and Pertlik, F. (1986) Four monazite type structures: comparison of $SrCrO_4$, $SrSeO_4$, $PbCrO_4$ (crocoite), and $PbSeO_4$. Zeitschrift für Kristallographie, 176, 75-83.

Ennaciri, A., Kahn, A., and Michel, D. (1986) Crystal structures of $HfGeO_4$ and $ThGeO_4$ germanates. Journal of the Less Common Metals, 124, 105-109.

Griffen, D. T. (1992) **Silicate Crystal Chemistry.** pp. 442, Oxford University Press.

Grumen, E., Daniels, E., and King, J. S. (1971) Crystal structure refinement of $SrMoO_4$, $SrWO_4$, $CaMoO_4$, and $BaWO_4$ by neutron diffraction. Journal of Chemical Physics, 55(3), 1093-1097.

Hassel, O. (1926) Die kristallstruktur einiger verbindugen von der zusammensetzung MRO_4 - I. Zircon $ZrSiO_4$. Zeitschrift für Kristallographie, 63, 247-254.

Hazen, R. M. and Finger, L. W. (1979) Crystal structure and compressibility of zircon at high pressure. American Mineralogist, 64, 196-201.

Henry, N. F. M. and Longsdale, K. eds. (1952) **The International Tables for X-Ray Crystallography vol. I: Symmetry Groups**. p. 558, The Kynoch Press.

Kalman, A., and Cruickshank, D. W. J. (1970) Refinement of the structure of $NaIO_4$. Acta Crystallographica, B26, 1782-1785.

Kay, M. I., Frazer, B. C., and Almodovar, I. (1964) Neutron diffraction refinement of $CaWO_4$. Journal of Chemical Physics, 40(2), 504-506.

Keller, C. (1963) Untersucheungen uber die germanate und silikate des typs ABO_4 der vierwertigen elemente thorium bis americium. Nukleonik, 5(2), 41-48.

Klebs, B., and Hasse, K. (1976) Refinement of the crystal structures of $KTcO_4$, $KReO_4$, and OsO_4. The bond lengths in tetrahedral oxo-anions and oxides of the d10 transition metals. Acta Crystallographica, B32, 1334-1337.

Knitte, E. and Williams, Q. (1993) High-Pressure raman spectroscopy of $ZrSiO_4$: observation of the zircon to scheelite transition at 300K. American Mineralogist, 78, 245-252.

Kokkoros, M. P. (1942) La structure de la monazite. Prakt. Athener Akad., 17, 163-174.

Kusaba, K, Syono, Y., Kikuchi, M., and Fukuoka, K. (1984) Shock behavior or zircon: phase transition to scheelite structure and decomposition. Earth and Planetary Science Letters, 72, 433-439.

Kusaba, K., Yagi, T., Kikuchi, M., and Syono, Y. (1986) Structural considerations on the mechanism of the shock-induced zircon-scheelite transition in $ZrSiO_4$. Journal of the Physics and Chemistry of Solids, 47(7), 675-679.

Leciejewicz, J. (1965) A neutron crystallographic investigation of lead molybdenum oxide, $PbMoO_4$. Zeitscrift für Kristallographie, 121, 158-164.

Lohmuller, V. G., Schmidt, G., Deppisch, B., Gramlich, V., and Scheringer, C. (1973) Die Kristallstrukturen von yittrium-vanadat, lutetium-phosphat, und lutetium-arsenat. Acta Crystallographica, B29, 141-142.

Long, F. G. and Stager, C. V. (1977) Low temperature crystal structure of $TbAsO_4$ and $DyAsO_4$. Canadian Journal of Physics, 55, 1633-1640.

Mashimo, T., Nagayama, K., and Sawaoka, A. (1983) Shock compression of Zirconia ZrO_2 and Zircon $ZrSiO_4$ in the pressure range up to 150 GPa. Physics and Chemistry of Minerals, 9, 237-247.

Miyake, M., Minato, I., Moriwaka, H., and Iwai, S. (1978) Crystal structures and sulphate force constants of barite, celestite, and anglesite. American Mineralogist, 63, 506-510.

Muller, O. and Roy, R. (1974) **Crystal Chemistry of Non-Metallic Materials Volume VI: The Major Ternary Structural Families**., pp. 487, Springer-Verlag, Berlin.

Mumpton, F. A. and Roy, R. (1961) Geochinica et Cosmochimica Acta, 21, 217-238.

Ni, Y., Hughes, J. M., and Mariano, A. N. (1995) Crystal chemistry of the monazite and xenotime structures. American Mineralogist, 80, 21-26.

O'Keeffe, M. and Hyde, B. G. (1981) The role of nonbonded forces in crystals. Structure and Bonding in Crystals, 1, 227-254.

O'Keeffe, M. and Hyde, B. G. (1985) An Alternative approach to non-molecular crystal structures. Structure and Bonding, 61, 77-144.

Patscheke, E., Fuess, H., and Will, G. (1968) Neutron diffraction study of $ErPO_4$ and $ErVO_4$. Chemical Physics Letters, 2(1), 47-49.

Pauling, L. (1929) Reviews in Physics B, 51, 1010-1026.

Range, K. and Meister, H. (1990) ErVO4-II, a scheelite type high-pressure modification of erbium orthovanadate. Acta Crystallographica, C46, 1093-1094.

Range, K., Meister, H., and Klement, U. (1990) Hochdruckumwandlungen von Cer(III)Orthovanadat(V), $CeVO_4$. Zeistscrift für Naturforsch., 45b, 598-602.

Reid, A. F., and Ringwood, A. E. (1969) Newly observed high-pressure transformations in Mn_3O_4, $CaAl_2O_4$, and $ZrSiO_4$. Earth and Planetary Science Letters, 6, 205-208.

Ribbe, P. H. and Macey, B. J. (1994) The zircon to scheelite transformation. GSA abstract.

Ribbe, P. H. and Prunier, A. R. (1977) Setereochemical analysis of ordered C2/c silicate pyroxenes. American Mineralogist, 62, 710-720.

Rice, C. E. and Robinson, R. R. (1976) Lanthanum orthovanadate. Acta Crystallographica, B32, 2232- 2233.

Robinson, K., Gibbs, G. V., and Ribbe, P. H. (1971) Quadratic elongation: a quantitative measure of distortion in coordination polyhedra. Science, 172, 567-570.

Schafer, W., Will, G., and Muller-Vogt, G. (1979) Refinement of the crystal structure of terbium arsenate $TbAsO_4$ at 77 K and 5 K by profile analysis from neutron diffraction powder data. Acta Crystallographica, B35, 588-592.

Shannon, R. D. (1976) Revised effective ionic radii and systematic studies of interatomic distances an halides and chalcogenides. Acta Crystallographica, A32, 751.

Sillen, L. G. and Nylander, A. L. (1943) Arkiv. Kemi. Geol., 17A(4).

Speer, J. A. and Cooper, B. J. (1982) Crystal structure of synthetic hafnon, $HfSiO_4$, comparison with zircon and the actinide orthosilicates. American Mineralogist, 67, 804-808.

Stubican, V. S. and Roy, R. (1963) High-pressure scheelite-structure polymorphs or rare-earth vanadates and arsenates. Zeitschrift für Kristalllographie, 119, 90-97.

Taylor, M. and Ewing, R. C. (1978) The crystal structures of the $ThSiO_4$ polymorphs: Huttonite and Thorite. Acta Crystallographica, B34, 1074-1079.

Vanderborre, M. T., Michel, D., and Ennaciri, A. (1989) Vibrational spectra and force fields of scheelite type germanates. Spectrochimica Acta, 45A(7), 721-727.

Vegard, L. (1926) Results of crystal analysis, part II, the zircon group. Philosophy Magazine, 7(1), 1158- 1168.

Wandahl, G. and Christensen, A. N. (1987) Neutron power diffraction profile refinement studies on $CaMoO_4$. A comparison with single crystal data. Acta Chemica Scandinavia A41, 358-360.

Zaslavskii, A. I. and Zvinchuk, R. A. (1953) Article in Russian. Dokladdy Akademii Nauk SSSR, 90, 781-783.

Computational Methods

Several computer programs were essential to the completion of this project. All the diagrams of crystal structures were created with XTALDRAW Demo version 4.13 (Boisen, Gibbs, Downs, Bartelmehs, 1990). These diagrams were saved as .pcx files and imported into PAINTBRUSH for editing. All calculations of crystal structure parameters was carried out with METRIC version 3.0 (Boisen, Gibbs, Downs, Bartelmehs, 1993). All regression equations were calculated with the statistical program JMP (Sail, John, Ng, Hect, Micheal, 1989-1991). All graphs were constructed using CRICKET GRAPH 1.3.2 (Rafferty and Norling, 1986-1989).

Preface to the Appendices

These appendices contain tables of structural parameters for compounds with the zircon-, scheelite-, and monazite-type structures. These parameters include: bond lengths (M-O and T-O), polyhedral volumes, bond angles (O-T-O, T-O-M and M-O-M), unit cell edge lengths, unit cell volume, tetrahedral quadratic elongation, and atomic positional parameters. The appendices also contain regression plots (observed parameter vs. calculated parameter) of these parameters as a function of rM, rT, and q. Appendix A contains data for zircon-type compounds. Four of these compounds have been excluded from the regression equations but included in the regression plots. These compounds are plotted as open circles (other data are plotted as closed circles or squares) and are labeled as follows: Dy = $DyAsO_4$, Tb = $TbAsO_4$, Lu = $LuAsO_4$, and Th = $ThSiO_4$ (thorite). Appendix B contains data for scheelite-type compounds. $ThGeO_4$ has been excluded from these regressions but is plotted (with an open circle) with the other data. Appendix C contains data for monazite-type compounds. $PbCrO_4$ (crocoite), $SrSeO_4$, and $ThSiO_4$ (huttonite) have been excluded from the regressions (in the same manner as the zircon- and scheelite-type compounds). These compounds are labeled as follows: Pb = $PbCrO_4$, Sr = $SrCrO_4$, and Th = $ThSiO_4$. They are plotted as open circles. These compounds have been excluded due to the consistent deviations they show in many of the regression plots.

Appendix A

REGRESSION PLOTS FOR ZIRCON-TYPE COMPOUNDS

Table A. Structural parameters for compounds with the zircon structure type.

Compound	T vol, Å^3	T-O, Å	TQE**	M-O1, Å	M-O2, Å	M vol, Å^3	O-T-O, °	T-O-M1, °	T-O-M2, °	M-O-M, °	a, Å	c, Å	Vol., Å^3	y	z	Ref.
$ZrSiO_4$	2.118	1.6229	1.0237	2.1286	2.2672	19.0044	96.966	149.84	99.107	111.053	6.6042	5.9796	260.803	0.066	0.195	A
$HfSiO_4$	2.1068	1.6202	1.0239	2.115	2.2599	18.7227	96.908	149.804	99.095	111.101	6.5725	5.9632	257.6	0.0655	0.1948	B
*$ThSiO_4$	2.2054	1.6346	1.0109	2.3676	2.4661	25.3243	100.972	153.66	98.76	107.58	7.1328	6.3188	321.48	0.0732	0.2104	C
*$DyAsO_4$	2.3765	1.6804	1.0164	2.3048	2.4256	23.7339	99.066	151.691	98.662	109.648	7.063	6.304	314.481	0.069	0.173	D
*$LuAsO_4$	2.3591	1.6737	1.0132	2.3175	2.4488	24.2524	100.126	152.664	98.332	109.003	7.09	6.32	317.694	0.069	0.17	E
*$LuAsO_4$	2.3722	1.6807	1.018	2.2483	2.3855	22.2832	98.55	151.085	98.452	110.463	6.949	6.227	300.693	0.0667	0.1989	F
$LuVO_4$	2.5019	1.7065	1.0129	2.2516	2.41	22.6633	100.239	152.024	96.967	111.009	7.0254	6.2347	307.721	0.0636	0.1995	G
$YbVO_4$	2.5067	1.7073	1.0125	2.2591	2.417	22.8778	100.365	152.152	96.96	110.888	7.0427	6.2472	309.859	0.0638	0.2	G
$TmVO_4$	2.5093	1.7081	1.0128	2.2721	2.4207	23.142	100.279	152.08	97.065	110.855	7.0682	6.2593	312.711	0.0645	0.2001	G
$ErVO_4$	2.5137	1.7091	1.0127	2.2853	2.4265	23.439	100.29	152.089	97.124	110.787	7.0957	6.2729	315.834	0.0651	0.2004	G
$HoVO_4$	2.5088	1.7079	1.0127	2.3003	2.4337	23.7859	100.308	152.147	97.147	110.609	7.1227	6.2891	319.064	0.0659	0.201	G
$TbVO_4$	2.5161	1.7093	1.0124	2.3269	2.451	24.4724	100.426	152.313	97.383	110.304	7.1774	6.3264	325.905	0.067	0.2021	G
$NdVO_4$	2.5259	1.7113	1.0121	2.4053	2.4984	26.5084	100.518	152.619	97.958	109.423	7.3308	6.4356	345.853	0.0705	0.205	G
$PrVO_4$	2.5294	1.7121	1.0121	2.4219	2.5108	26.9863	100.521	152.701	98.115	109.184	7.3631	6.465	350.502	0.0712	0.2057	G
$CeVO_4$	2.527	1.7114	1.012	2.4421	2.5254	27.5655	100.576	152.842	98.292	108.866	7.4004	6.4972	355.825	0.0721	0.2067	G
YVO_4	2.5114	1.7087	1.0129	2.298	2.4327	23.7324	100.238	152.092	97.266	110.642	7.1183	6.2893	318.68	0.0658	0.2008	G
$ScVO_4$	2.4921	1.7044	1.0131	2.1289	2.3671	20.1768	100.158	152.005	96.398	111.598	6.78	6.1345	282.01	0.0572	0.1967	G
$LuPO_4$	1.8329	1.5339	1.007	2.2575	2.3438	21.8528	102.646	154.851	97.951	107.199	6.7848	5.9467	273.747	0.0735	0.2138	H
$YbPO_4$	1.8268	1.5318	1.0065	2.2703	2.3553	22.1937	102.937	155.144	97.951	106.905	6.8083	5.9639	276.444	0.074	0.215	H
$TmPO_4$	1.9089	1.5545	1.0065	2.2612	2.3586	22.114	102.9	154.907	97.524	107.569	6.8297	5.9798	278.927	0.072	0.213	H
$ErPO_4$	1.8421	1.5356	1.0059	2.2878	2.3729	22.6969	103.233	155.416	97.901	106.687	6.851	5.9968	281.467	0.0743	0.216	H
$HoPO_4$	1.8273	1.5319	1.0064	2.3066	2.3791	23.0751	102.982	155.302	98.254	106.445	6.8772	6.0176	284.608	0.0757	0.2165	H
$PrPO_4$	1.8454	1.5372	1.0067	2.3173	2.385	23.3325	102.901	155.153	98.348	106.499	6.9046	6.0384	287.872	0.076	0.2162	H
$TbPO_4$	1.8431	1.536	1.006	2.331	2.3993	23.7392	103.156	155.494	98.32	106.186	6.9319	6.0606	291.219	0.0764	0.2175	H
YPO_4	1.8675	1.5435	1.007	2.3001	2.3729	22.908	102.643	154.894	98.161	106.945	6.8817	6.0177	284.985	0.0749	0.2147	I
$ScPO_4$	1.8254	1.5341	1.01	2.1535	2.2598	19.2835	101.337	153.423	97.657	108.92	6.574	5.791	250.272	0.0695	0.2071	I

* These compounds have been excluded from the calculation of the regression equations, but are included in plots of the regression equations.
** Tetrahedral quadratic elongation, as defined by Robinson, Gibbs, and Ribbe (1971).

A - Hazen and Finger (1979)
B - Speer and Cooper (1982)
C - Taylor and Ewing (1978)
D - Long and Stager (1977)
E - Schafer, Will, and Muller-Vogt (1979)
F - Lohmuller, Schmidt, Deppisch, Gramich, and Scheringer (1973)
G - Chakoumakos, Abraham, and Boatner (1994)
H - Ni, Hughes, and Mariano (1995)
I - Milligan, Mullica, Beal, and Boatner (1982)

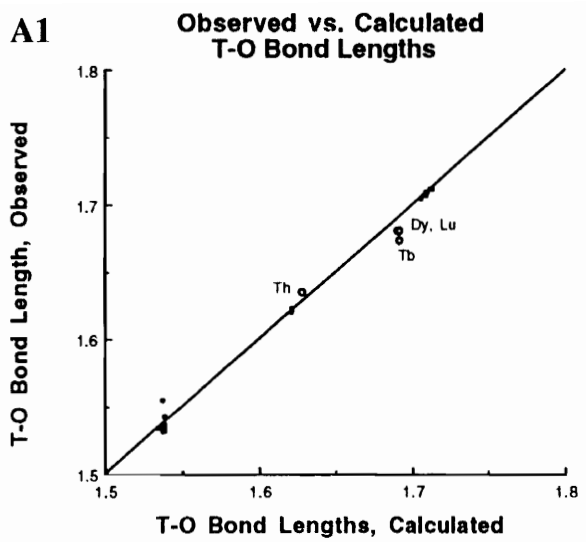
A1
Observed vs. Calculated
T-O Bond Lengths
T-O Bond Length, Observed
T-O Bond Lengths, Calculated
1.5
1.6
1.7
1.8
Th
Dy, Lu
Tb

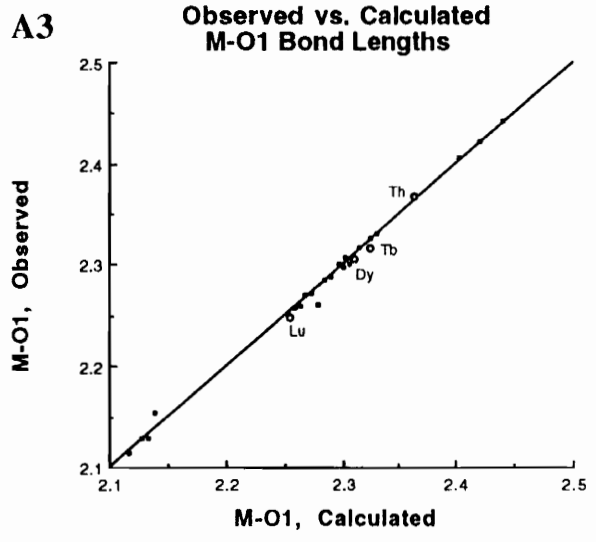
A3
Observed vs. Calculated
M-O1 Bond Lengths
M-O1, Observed
M-O1, Calculated
2.1
2.2
2.3
2.4
2.5
Th
Tb
Dy
Lu

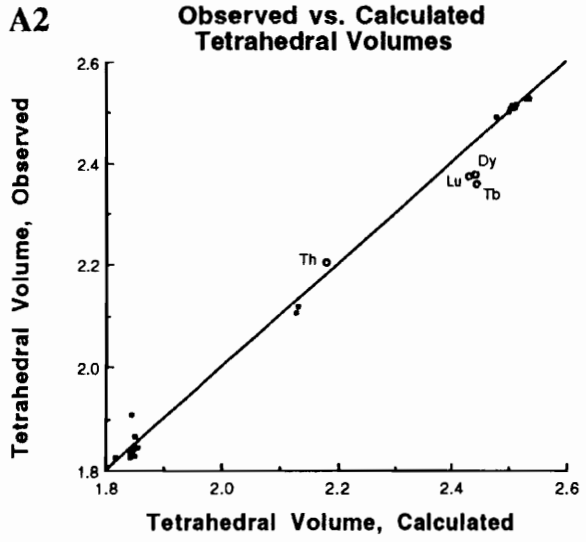
A2
Observed vs. Calculated
Tetrahedral Volumes
Tetrahedral Volume, Observed
Tetrahedral Volume, Calculated
1.8
2.0
2.2
2.4
2.6
Th
Dy
Lu
Tb

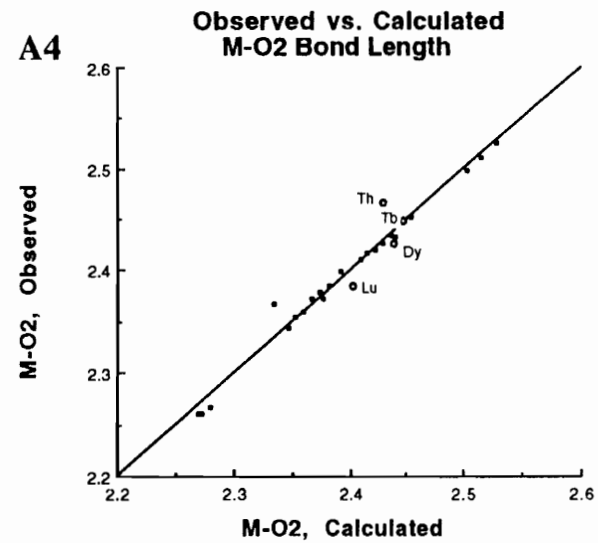
A4
Observed vs. Calculated
M-O2 Bond Length
M-O2, Observed
M-O2, Calculated
2.2
2.3
2.4
2.5
2.6
Th
Tb
Dy
Lu

A5

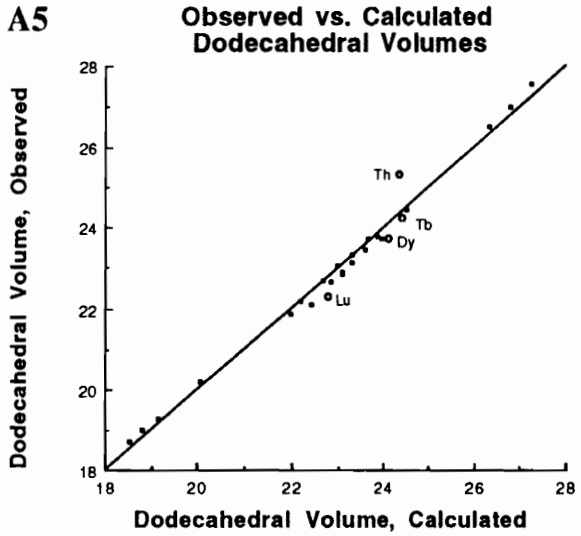
Observed vs. Calculated
Dodecahedral Volumes
Dodecahedral Volume, Observed
Dodecahedral Volume, Calculated
Th
Tb
Dy
Lu
18
20
22
24
26
28

A7

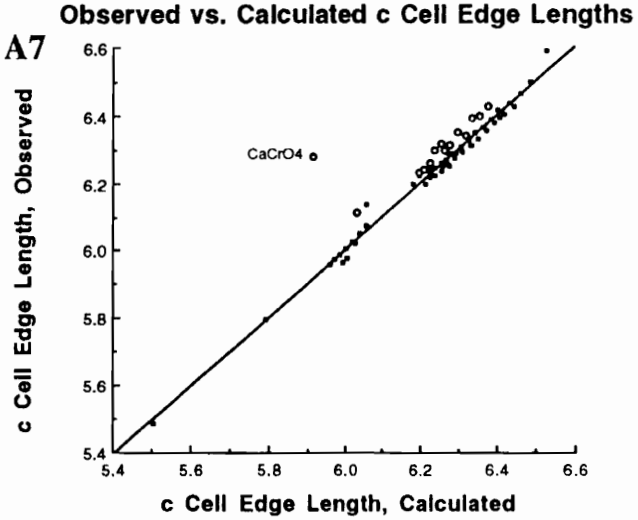
Observed vs. Calculated c Cell Edge Lengths
c Cell Edge Length, Observed
c Cell Edge Length, Calculated
CaCrO4
5.4
5.6
5.8
6.0
6.2
6.4
6.6

A6

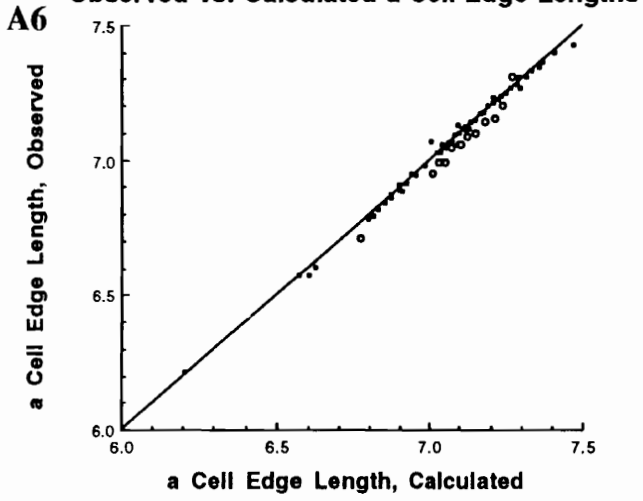
Observed vs. Calculated a Cell Edge Lengths
a Cell Edge Length, Observed
a Cell Edge Length, Calculated
6.0
6.5
7.0
7.5

A8

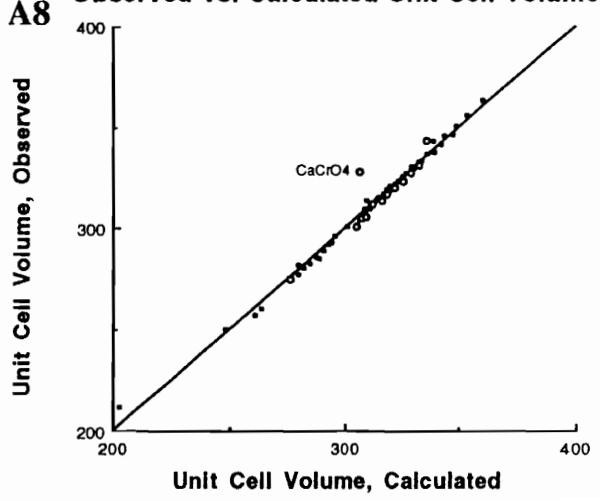
Observed vs. Calculated Unit Cell Volumes
Unit Cell Volume, Observed
Unit Cell Volume, Calculated
CaCrO4
200
300
400

A9

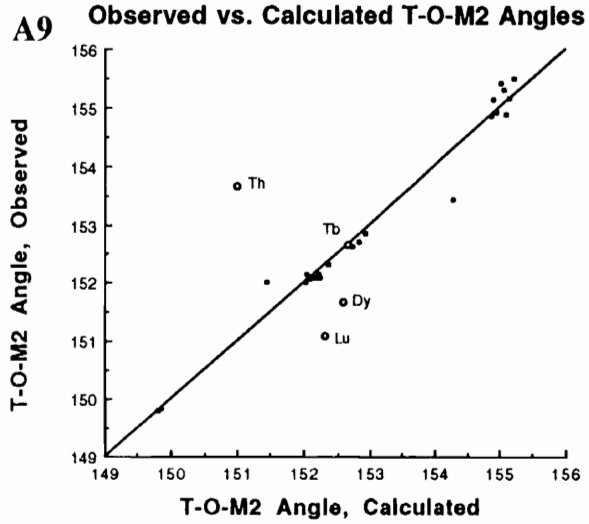

A11

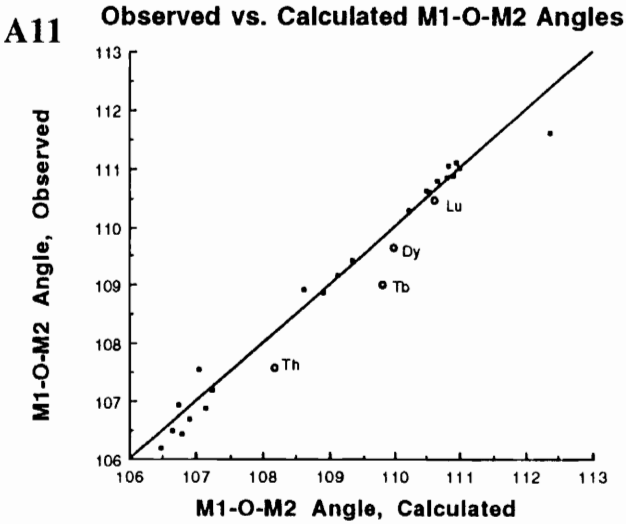

A10

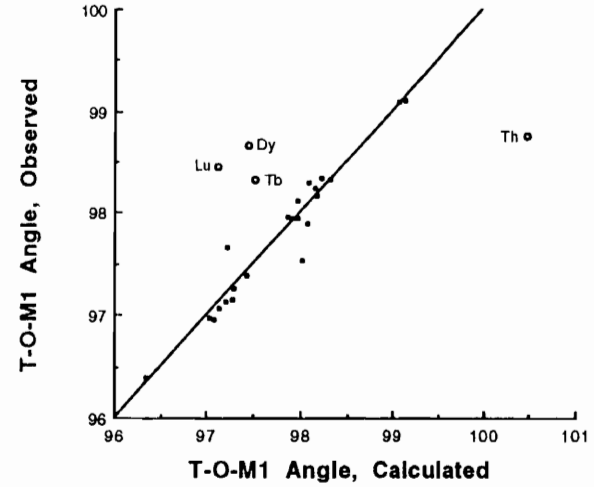

A12

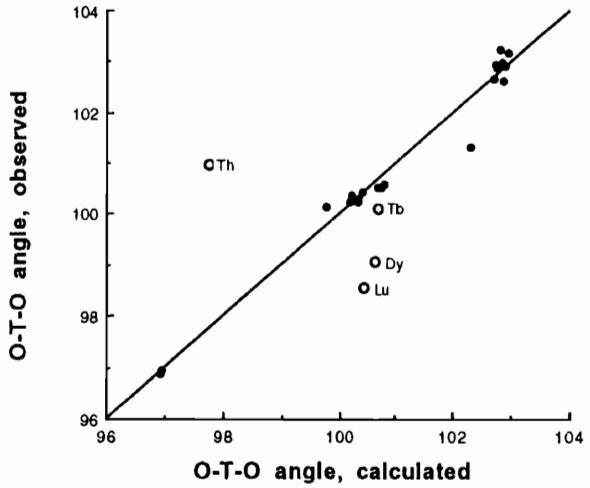

A13

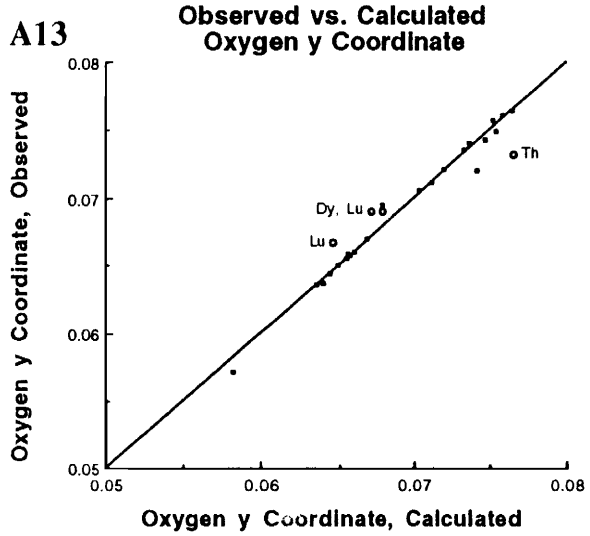
Observed vs. Calculated
Oxygen y Coordinate
Oxygen y Coordinate, Observed
Oxygen y Coordinate, Calculated
0.05
0.06
0.07
0.08
Th
Dy, Lu
Lu

A15

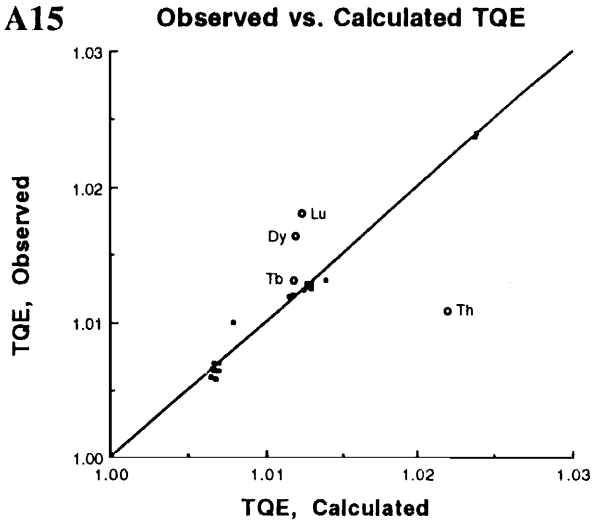
Observed vs. Calculated TQE
TQE, Observed
TQE, Calculated
1.00
1.01
1.02
1.03
Lu
Dy
Tb
Th

A14

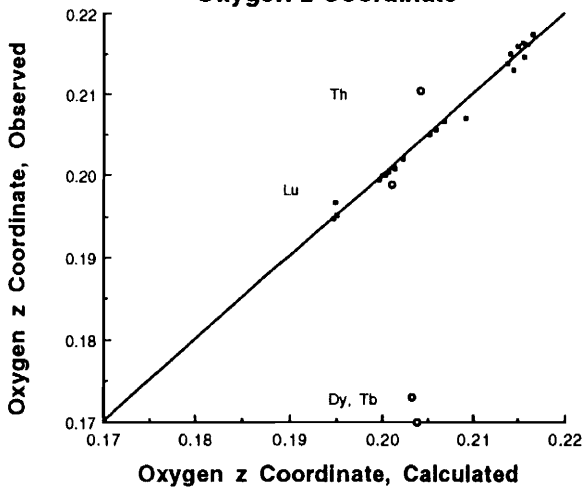
Observed vs. Calculated
Oxygen z Coordinate
Oxygen z Coordinate, Observed
Oxygen z Coordinate, Calculated
0.17
0.18
0.19
0.20
0.21
0.22
Th
Lu
Dy, Tb

Appendix B

REGRESSION PLOTS FOR SCHEELITE-TYPE COMPOUNDS

Table B. Structural parametrs of compound with the scheelite structure type.

Comp.	O-T-O, °	T vol, Å^3	T-O, Å	TQE**	M-O1	M-O2	M vol,Å^3	T-O-M1, °	T-O-M2, °
β-ErVO	105.713	2.5815	1.7216	1.0095	2.3327	2.368	23.0784	131.915	120.774
$CaWO_4$	107.516	2.9099	1.7854	1.0024	2.438	2.479	26.3758	132.037	119.893
$CaMoO_4$	107.098	2.8538	1.7749	1.0036	2.4474	2.4657	26.3429	132.27	120.237
$PbMoO_4$	107.842	2.8568	1.7738	1.0017	2.6077	2.6321	32.0205	135.418	120.044
$KReO_4$	108.939	2.6634	1.7315	1.0002	2.7835	2.8662	40.2083	140.372	119.77
$ZrGeO_4$	103.871	2.7592	1.7715	1.0225	2.1407	2.2655	18.7698	125.034	122.889
$HfGeO_4$	103.884	2.8032	1.7808	1.0224	2.1329	2.2492	18.4523	124.756	122.658
*$ThGeO_4$	103.256	2.5512	1.7308	1.0284	2.3315	2.3525	23.0511	129.356	125.303
$SrWO_4$	107.579	2.8724	1.7775	1.0023	2.5777	2.6082	31.0504	134.613	120.396
$SrMoO_4$	107.636	2.8201	1.7665	1.0021	2.5831	2.61	31.2013	135.489	120.013
$BaWO_4$	108.106	2.8998	1.7822	1.0012	2.7387	2.7783	37.4611	138.568	119.443
$NaIO_4$	107.232	2.8281	1.7692	1.0032	2.5354	2.5984	29.925	132.069	121.471
$KTcO_4$	108.971	2.5682	1.7106	1.0002	2.7936	2.8642	40.3944	142.102	118.787

Comp.	M-O-M, °	a, Å	c, Å	Vol, Å^3	x	y	z	Ref
β-ErVO	105.587	5.003	11.143	278.90	0.245	0.146	0.0446	A
$CaWO_4$	103.742	5.243	11.376	312.715	0.2587	0.1511	0.0861	B
$CaMoO_4$	103.973	5.2225	11.4298	311.742	0.2564	0.149	0.0842	C
$PbMoO_4$	101.8	5.4312	12.1065	357.117	0.2352	0.1134	0.0439	D
$KReO_4$	97.952	5.6817	12.7118	410.364	0.2785	0.1169	0.0474	E
$ZrGeO_4$	109.035	4.866	10.552	249.85	0.2332	0.171	0.0815	F
$HfGeO_4$	109.41	4.862	10.497	248.14	0.2322	0.1739	0.0831	F
*$ThGeO_4$	103.599	5.145	10.531	278.77	0.2452	0.1493	0.0787	G
$SrWO_4$	101.989	5.4136	11.942	349.985	0.2638	0.1395	0.0818	H
$SrMoO_4$	102.056	5.3936	12.019	349.644	0.2626	0.1357	0.0809	H
$BaWO_4$	100.51	5.6148	12.721	401.042	0.2668	0.1227	0.0781	H
$NaIO_4$	102.545	5.337	11.947	340.293	0.2659	0.1501	0.0806	I
$KTcO_4$	98.134	5.63	12.867	407.844	0.2754	0.1089	0.0492	J

* These compounds have been excluded from the calculation of the regression equations, but are included in plots of the regression equations.
** Tetrahedral quadratic elongation, as defined by Robinson, Gibbs, and Ribbe (1971).

A - Range and Meister (1990)
B - Kay, Frazier, and Almodovar (1964)
C - Wandahl and Christensen (1987)
D - Leciejewicz (1965)
E - Brown, Powell, and Stuart (1993)
F - Vandenborre, Michel, and Ennaciri (1989)
G - Ennaciri, Kahn, and Michel (1986)
H - Gurmen, Daniels, and King (1971)
I - Kalman and Cruickshank (1970)
J - Klebs and Hasse (1976)

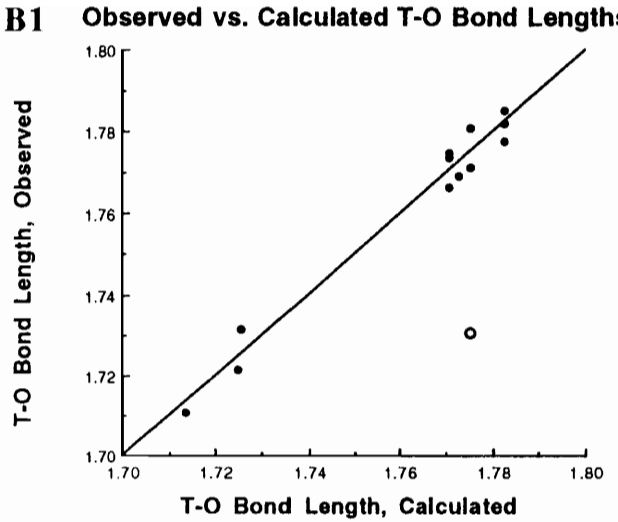
B1
Observed vs. Calculated T-O Bond Lengths
T-O Bond Length, Observed
T-O Bond Length, Calculated
1.70
1.72
1.74
1.76
1.78
1.80

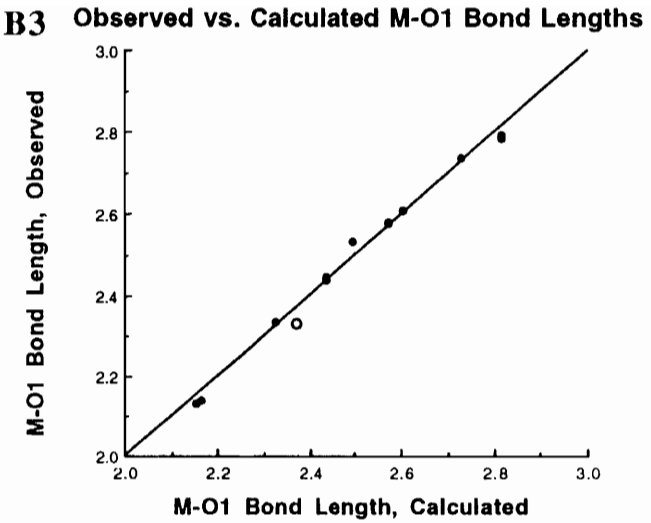
B3
Observed vs. Calculated M-O1 Bond Lengths
M-O1 Bond Length, Observed
M-O1 Bond Length, Calculated
2.0
2.2
2.4
2.6
2.8
3.0

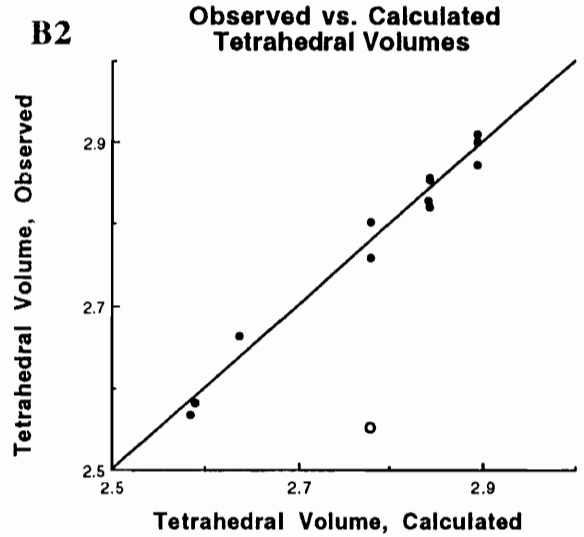
B2
Observed vs. Calculated
Tetrahedral Volumes
Tetrahedral Volume, Observed
Tetrahedral Volume, Calculated
2.5
2.7
2.9

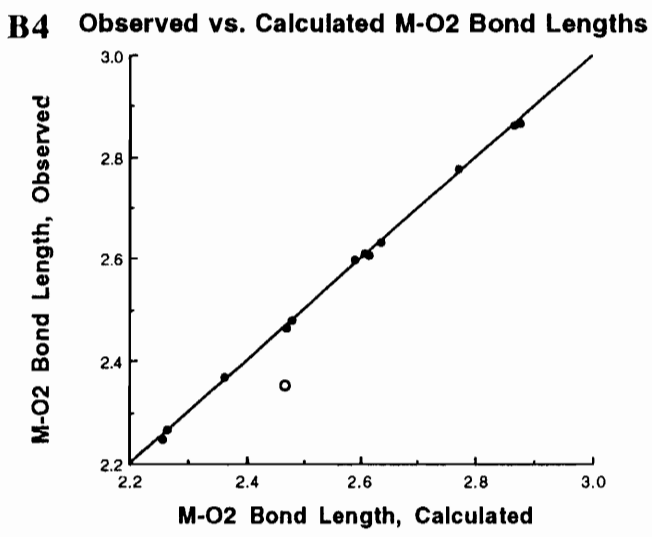
B4
Observed vs. Calculated M-O2 Bond Lengths
M-O2 Bond Length, Observed
M-O2 Bond Length, Calculated
2.2
2.4
2.6
2.8
3.0

B5 Observed vs. Calculated Dodecahedral Volumes

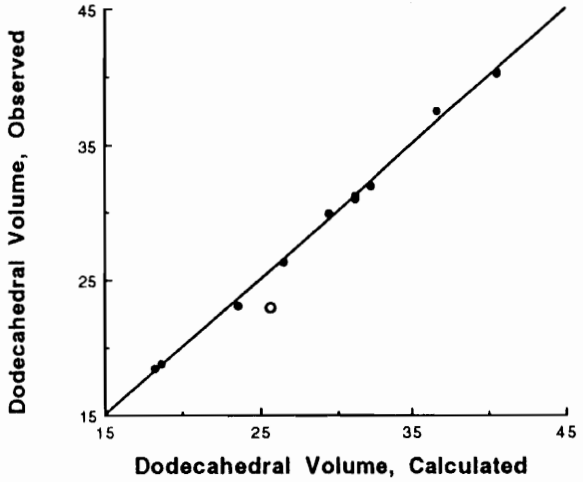

B7 Observed vs. Calculated c Cell Edge Lengths

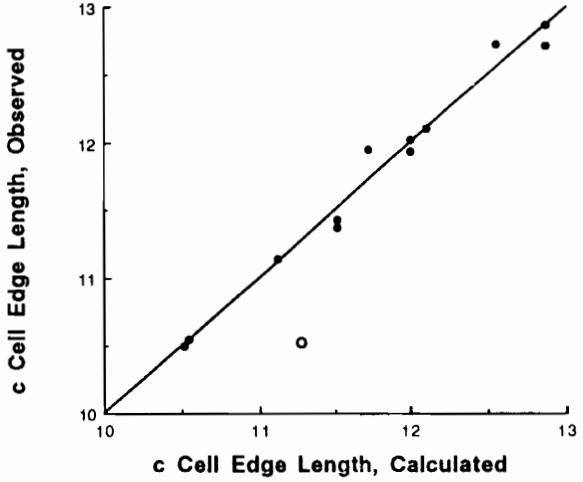

B6 Observed vs. Calculated a Cell Edge Lengths

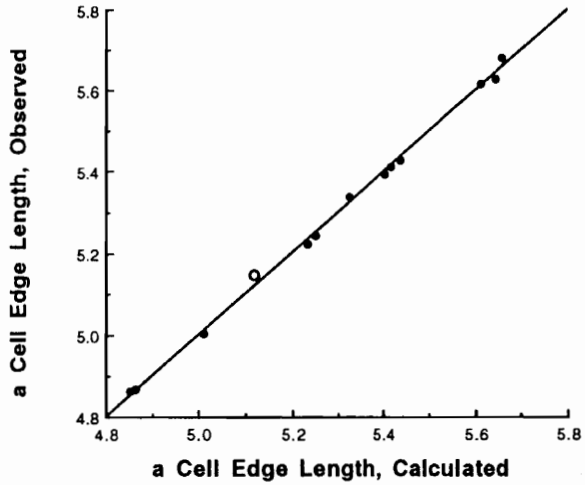

B8 Observed vs. Calculated Unit Cell Volumes

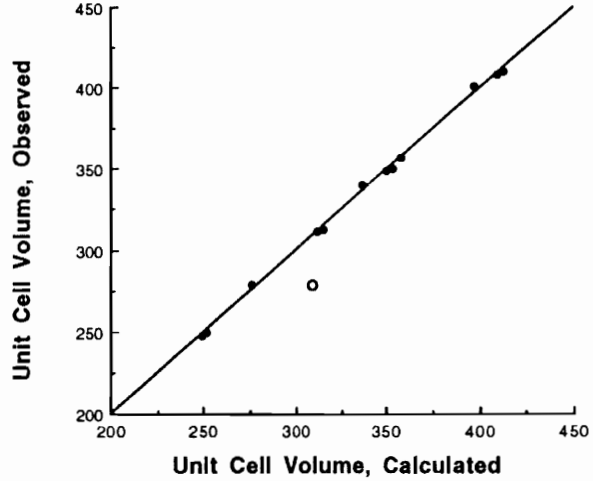

B9

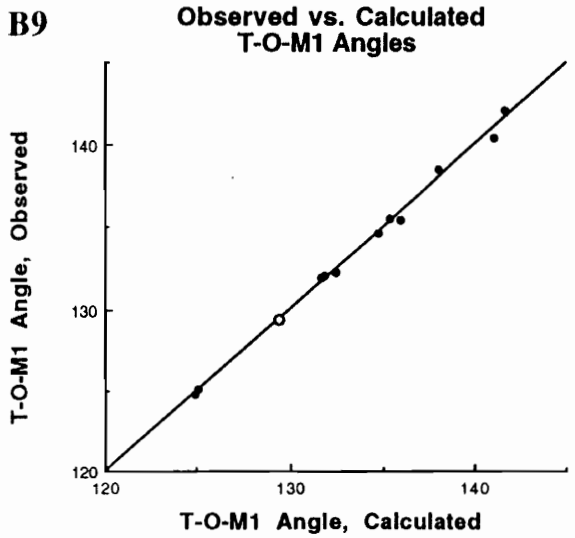

B11

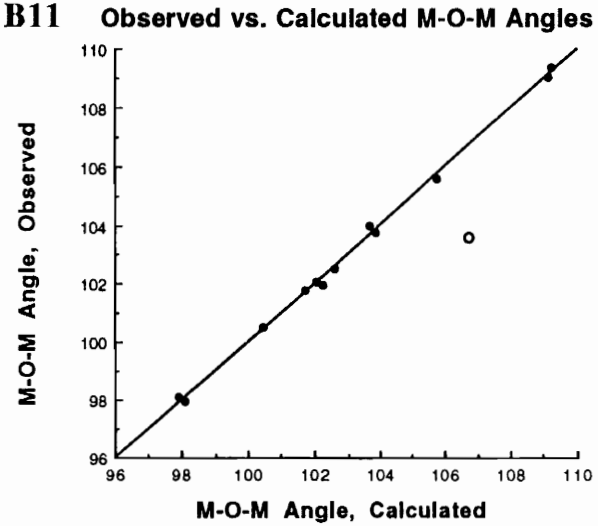

B10

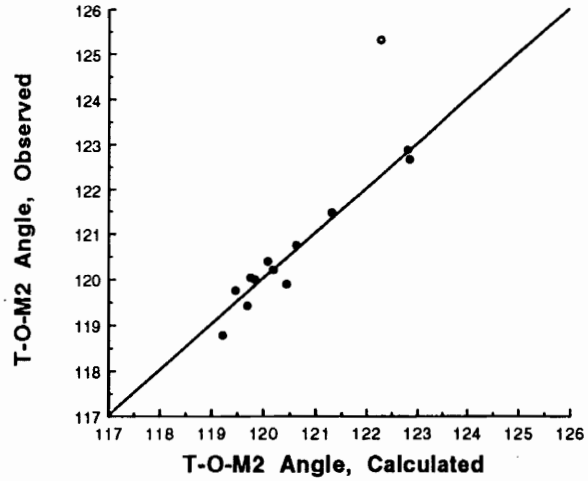

B12

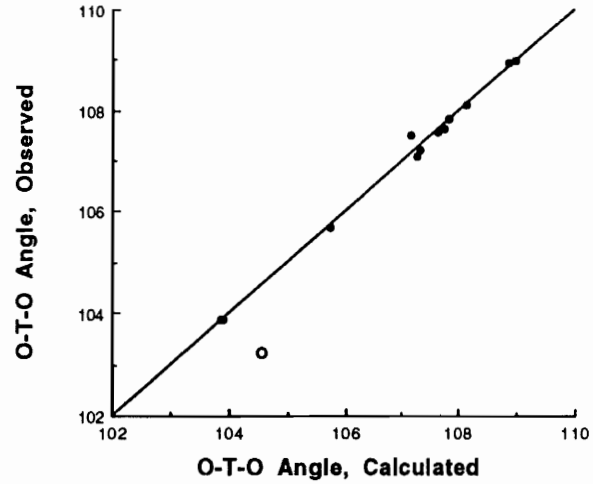

B13

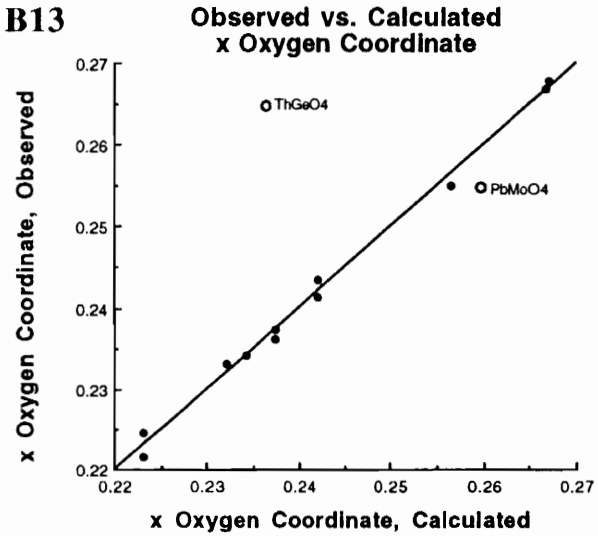
Observed vs. Calculated
x Oxygen Coordinate
x Oxygen Coordinate, Observed
x Oxygen Coordinate, Calculated
ThGeO4
PbMoO4
0.22
0.23
0.24
0.25
0.26
0.27

B15

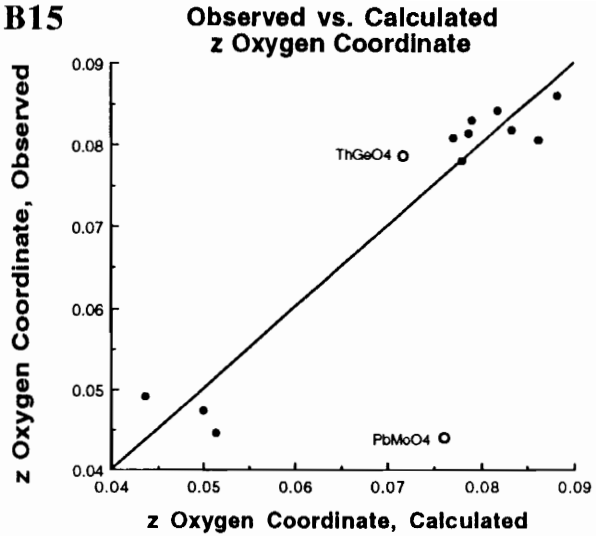
Observed vs. Calculated
z Oxygen Coordinate
z Oxygen Coordinate, Observed
z Oxygen Coordinate, Calculated
ThGeO4
PbMoO4
0.04
0.05
0.06
0.07
0.08
0.09

B14

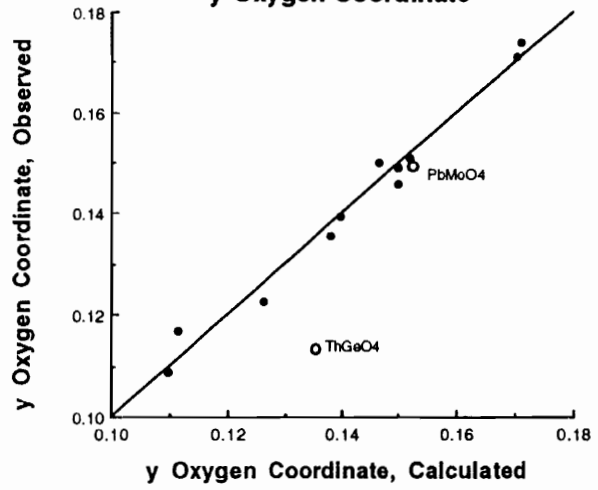
Observed vs. Calculated
y Oxygen Coordinate
y Oxygen Coordinate, Observed
y Oxygen Coordinate, Calculated
PbMoO4
ThGeO4
0.10
0.12
0.14
0.16
0.18

Appendix C

REGRESSION PLOTS FOR MONAZITE-TYPE COMPOUNDS

Table C. Oxygen positional parameters for monazite-type compounds

Name	xM	yM	zM	xT	yT	zT	xO1	yO1	zO1	xO2
$GdPO_4$	0.18455	0.15529	0.2815	0.69	0.1612	0.3031	0.1846	0.5013	0.2461	0.1187
$EuPO_4$	0.18395	0.15595	0.28152	0.6899	0.1615	0.3029	0.1896	0.5012	0.2487	0.1184
$SmPO_4$	0.1834	0.15538	0.28153	0.6904	0.1618	0.3034	0.1906	0.502	0.2501	0.1186
$NdPO_4$	0.18228	0.15580	0.28178	0.691	0.1626	0.3037	0.1928	0.5046	0.2498	0.1172
$PrPO_4$	0.18189	0.15586	0.28177	0.6913	0.163	0.304	0.1943	0.5051	0.2502	0.1174
$CePO_4$	0.18174	0.15591	0.28182	0.6923	0.1635	0.3047	0.195	0.5055	0.2492	0.1171
$LaPO_4$	0.18086	0.16033	0.28154	0.692	0.1639	0.3047	0.1974	0.5077	0.2503	0.1165
$SrCrO_4$	0.1699	0.15869	0.27187	0.6892	0.16487	0.3023	0.2022	0.5055	0.2584	0.1177
$PbCrO_4$*	0.17562	0.14549	0.2787	0.6807	0.16364	0.2989	0.1964	0.5042	0.2538	0.1355
$SrSeO_4$*	0.17794	0.15773	0.27918	0.69224	0.1651	0.30636	0.1932	0.5052	0.2516	0.1158
$LaVO_4$	0.17269	0.15725	0.27633	0.68561	0.16465	0.30055	0.1828	0.4987	0.2435	0.109
$ThSiO_4$*	0.184	0.155	0.2828	0.6903	0.1616	0.302	0.1825	0.4976	0.2549	0.1067
β-$CeVO_4$	0.17239	0.15657	0.27561	0.68492	0.1647	0.30052	0.181	0.4959	0.2541	0.1111

Name	yO2	zO2	xO3	yO3	zO3	xO4	yO4	zO4	a, Å	b, Å
$GdPO_4$	-0.1654	0.1183	0.6603	0.1016	0.4729	0.4056	0.2138	0.1187	6.3281	6.8414
$EuPO_4$	-0.165	0.1167	0.6627	0.1022	0.4743	0.4085	0.2135	0.1204	6.3491	6.8618
$SmPO_4$	-0.1659	0.1178	0.6646	0.1025	0.4748	0.4104	0.2125	0.1217	6.3653	6.8827
$NdPO_4$	-0.1669	0.1185	0.6674	0.104	0.4747	0.4122	0.2153	0.1249	6.4049	6.95
$PrPO_4$	-0.1673	0.1184	0.6687	0.1046	0.4744	0.414	0.215	0.126	6.4344	6.9812
$CePO_4$	-0.168	0.1189	0.6703	0.1054	0.4745	0.416	0.2164	0.1268	6.465	7.0163
$LaPO_4$	-0.1685	0.1201	0.673	0.1071	0.4748	0.4176	0.2168	0.1277	6.5034	7.0705
$SrCrO_4$	-0.1627	0.1201	0.6725	0.1012	0.4744	0.4105	0.2179	0.1224	6.741	7.375
$PbCrO_4$*	-0.1575	0.1245	0.6563	0.0999	0.5295	0.396	0.2141	0.1141	6.799	7.438
$SrSeO_4$*	-0.1625	0.1154	0.6743	0.1094	0.4808	0.412	0.2167	0.1141	6.874	7.34
$LaVO_4$	-0.1566	0.1136	0.6576	0.1056	0.4815	0.3908	0.2203	0.118	6.725	7.286
$ThSiO_4$*	-0.1612	0.11	0.6569	0.106	0.4803	0.3971	0.2122	0.1216	6.5	6.974
β-$CeVO_4$	-0.1544	0.1124	0.6575	0.1052	0.4832	0.3816	0.222	0.1106	6.685	7.227

Name	c, Å	β, °	TQE**	M-O, Å	T-O, Å	M vol, $Å^3$	T vol, $Å^3$	T-O1-M1, °	T-O1-M2, °	M-O-M, °	Ref
$GdPO_4$	7.9921	126.23	1.006	2.476	1.5383	29.5275	1.8516	111.748	140.843	106.292	A
$EuPO_4$	8.0177	126.26	1.005	2.4879	1.5378	29.9496	1.8525	111.133	141.824	105.571	A
$SmPO_4$	8.049	126.3	1.0048	2.4982	1.5366	30.3321	1.8487	111.056	141.702	105.519	A
$NdPO_4$	8.1229	126.33	1.0048	2.5242	1.5371	31.2723	1.8505	110.394	142.465	105.359	A
$PrPO_4$	8.1692	126.327	1.0045	2.5406	1.5375	31.8937	1.8528	110.108	142.841	105.155	A
$CePO_4$	8.2151	126.52	1.004	2.5554	1.5374	32.4329	1.8539	109.792	143.472	104.922	A
$LaPO_4$	8.2804	126.58	1.0038	2.5784	1.5392	33.3073	1.8608	109.310	143.682	104.932	A
$SrCrO_4$	8.5906	126.77	1.0134	2.6693	1.626	36.8499	2.1991	109.346	142.968	104.159	B
$PbCrO_4$*	8.727	127.106	1.0022	2.683	1.6633	37.6865	2.3525	108.419	142.004	107.438	B
$SrSeO_4$*	8.6556	127.08	1.0032	2.6857	1.6462	37.5025	2.2786	109.239	142.988	105.976	B
$LaVO_4$	8.402	125.834	1.011	2.5965	1.709	33.7159	2.5203	113.752	139.101	104.863	C
$ThSiO_4$*	8.0972	125.95	1.0134	2.507	1.6163	30.4128	2.1244	112.232	141.571	105.345	D
β-$CeVO_4$	8.3242	125.697	1.0102	2.571	1.7183	32.7405	2.5651	114.022	139.606	104.519	E

A - Ni, Hughes, and Mariano (1995)
B - Effenberger and Pertlik (1986)
C - Rice and Robinson (1976)
D - Taylor and Ewing (1978)
E - Range, Meister, and Klement (1989)

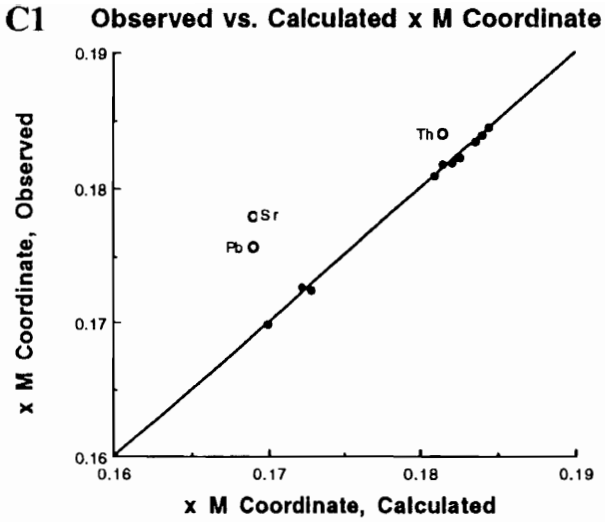
C1
Observed vs. Calculated x M Coordinate
x M Coordinate, Observed
x M Coordinate, Calculated
0.19
0.18
0.17
0.16
0.16
0.17
0.18
0.19
Th
Sr
Pb

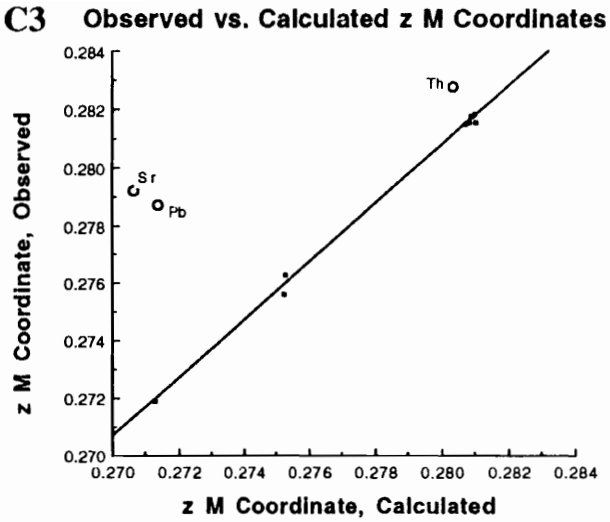
C3
Observed vs. Calculated z M Coordinates
z M Coordinate, Observed
z M Coordinate, Calculated
0.284
0.282
0.280
0.278
0.276
0.274
0.272
0.270
0.270
0.272
0.274
0.276
0.278
0.280
0.282
0.284
Th
Sr
Pb

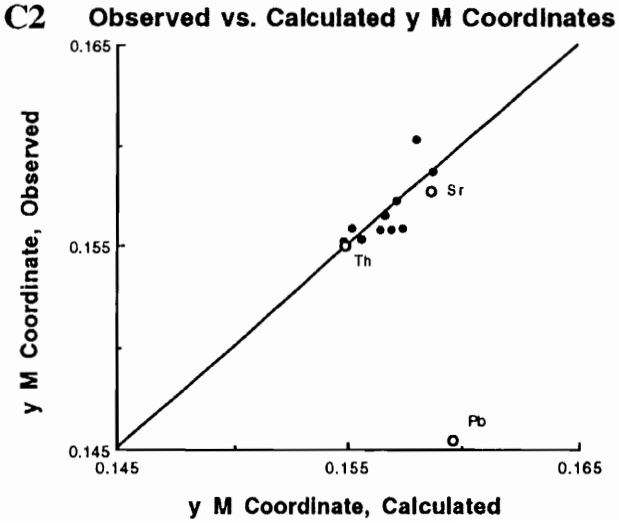
C2
Observed vs. Calculated y M Coordinates
y M Coordinate, Observed
y M Coordinate, Calculated
0.165
0.155
0.145
0.145
0.155
0.165
Sr
Th
Pb

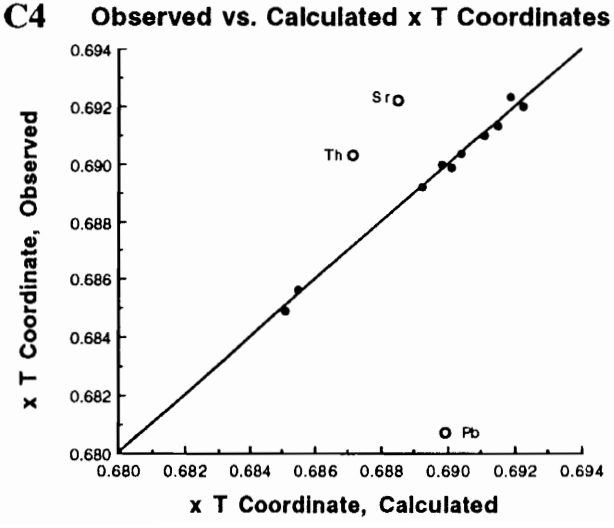
C4
Observed vs. Calculated x T Coordinates
x T Coordinate, Observed
x T Coordinate, Calculated
0.694
0.692
0.690
0.688
0.686
0.684
0.682
0.680
0.680
0.682
0.684
0.686
0.688
0.690
0.692
0.694
Sr
Th
Pb

C5 Observed vs. Calculated y T Coordinate

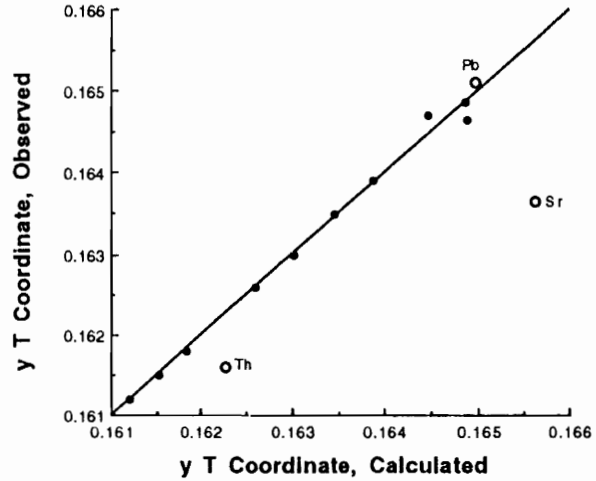

C7 Observed vs. Calculated x O1 Coordinates

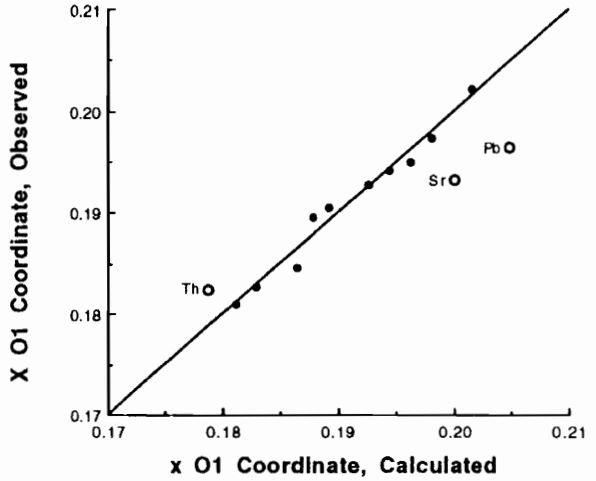

C6 Observed vs. Calculated z T Coordinate

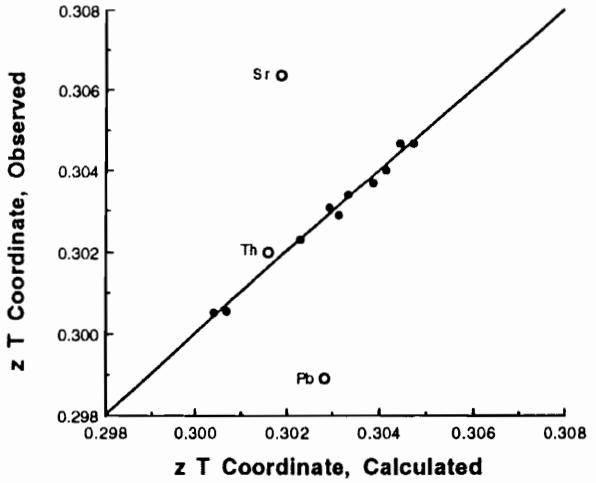

C8 Observed vs. Calculated y O1 Coordinate

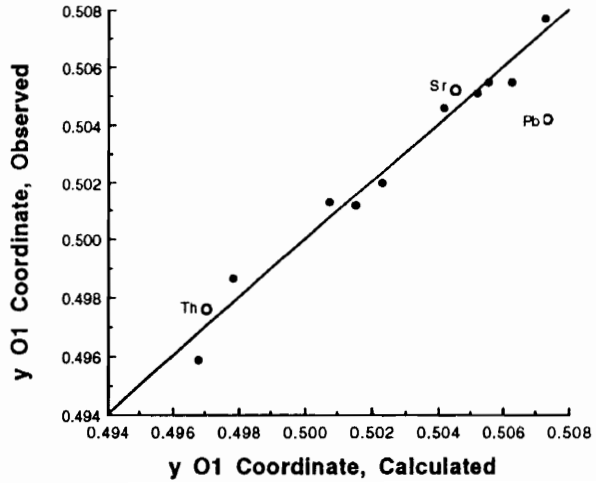

C9 Observed vs. Calculated z O1 Coordinates

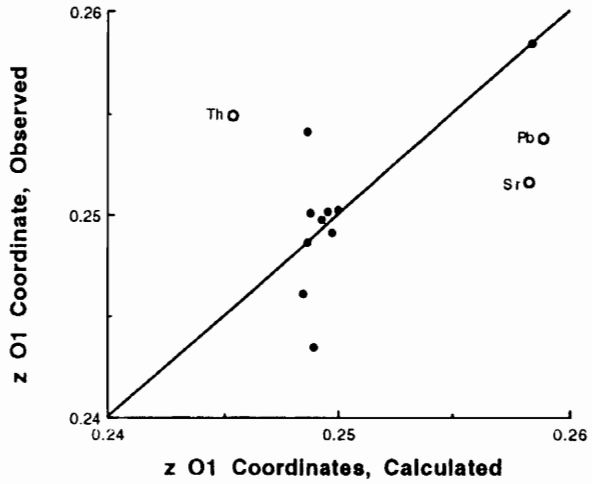

C11 Observed Vs. Calculated y O2 Coordinates

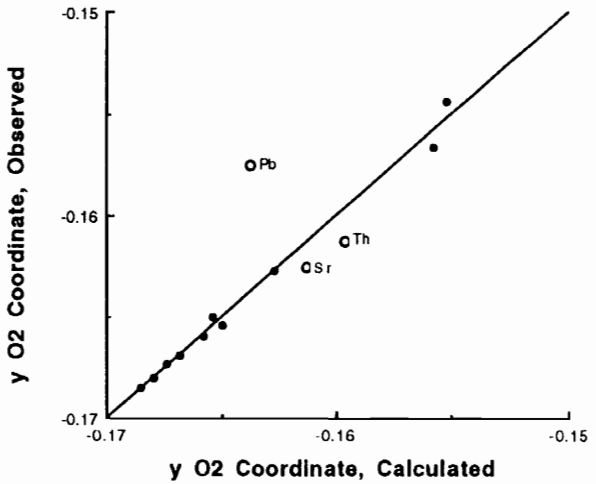

C10 Observed vs. Calculated x O2 Coordinates

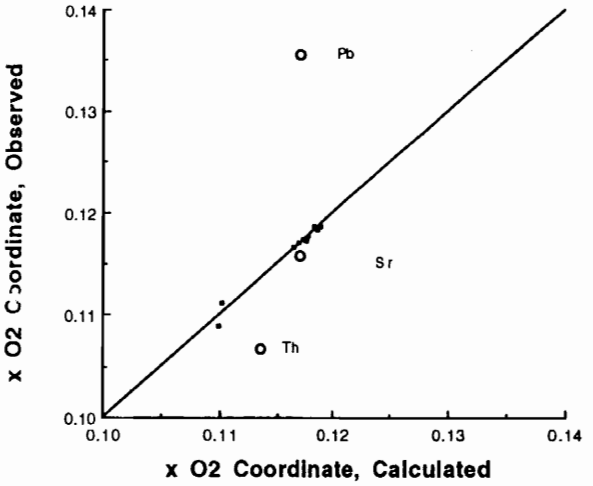

C12 Observed vs. Calculated z O2 Coordinates

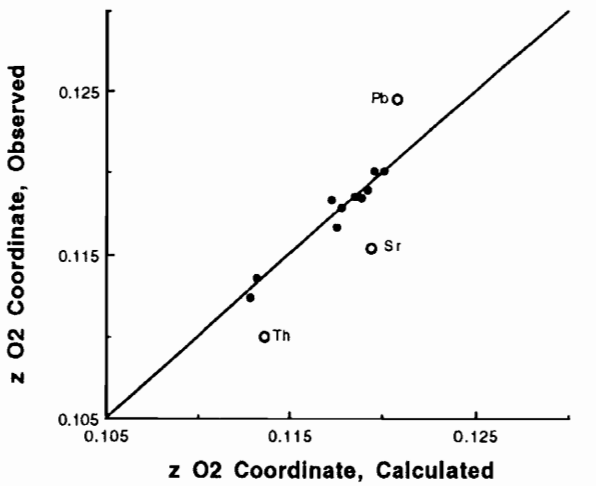

C13 **Observed vs. Calculated x O3 Coordinates**

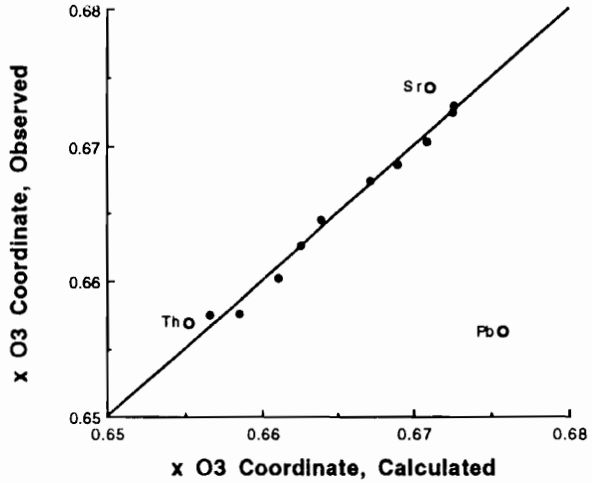

C15 Observed vs. Calculated z O3 Coordinate

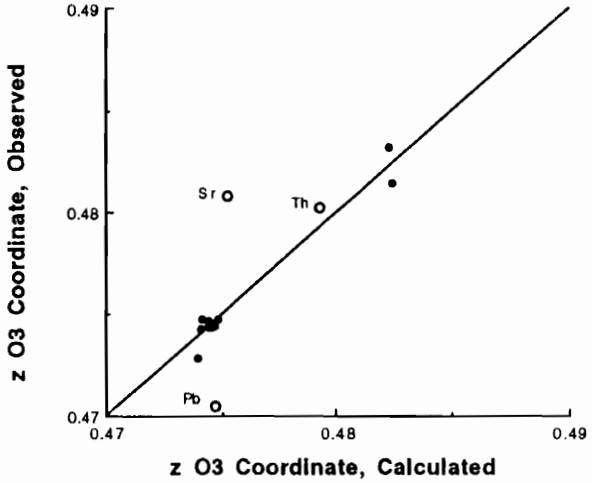

C14 **Observed vs. Calculated y O3 Coordinates**

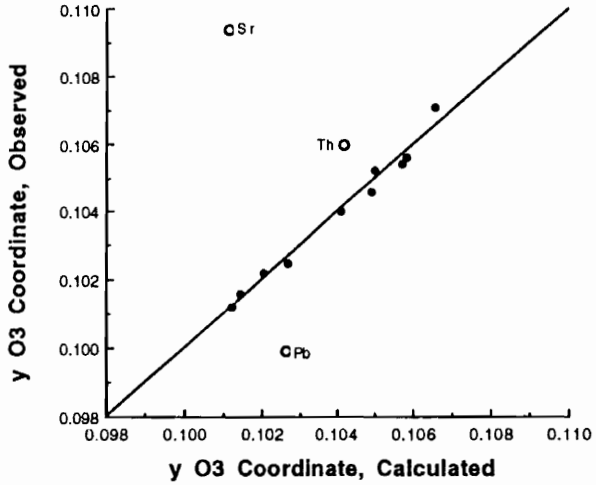

C16 **Observed vs. Calculated x O4 Coordinates**

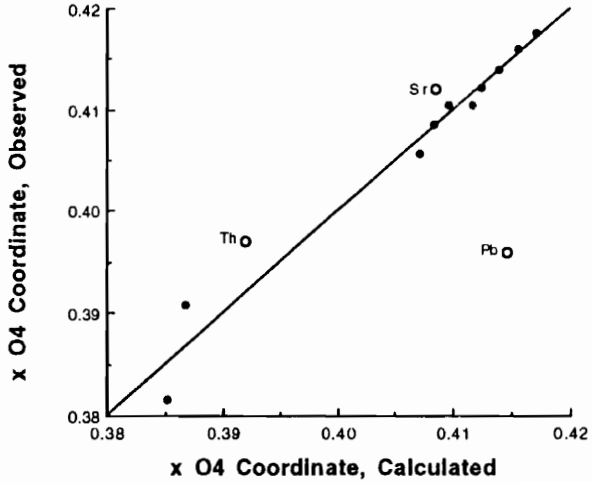

C17 Observed vs. Calculated y O4 Coordinates

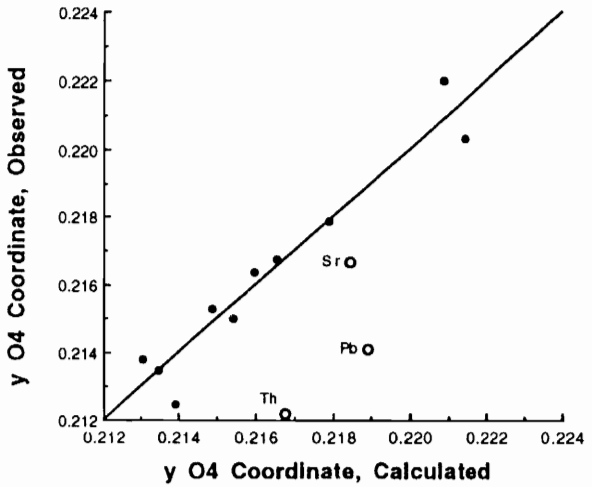

C19 Observed vs. Calculated Average T-O Bond Lengths

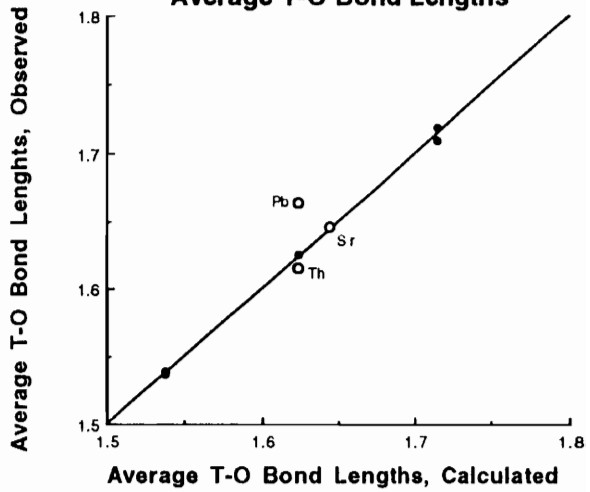

C18 Observed vs. Calculated z O4 Coordinates

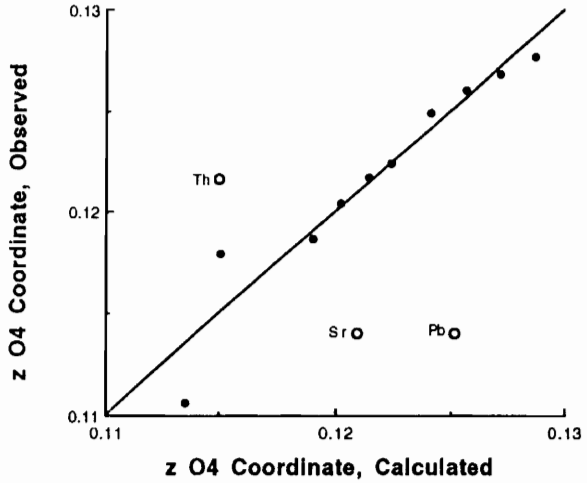

C20 Observed vs. Calculated Tetrahedral Volumes

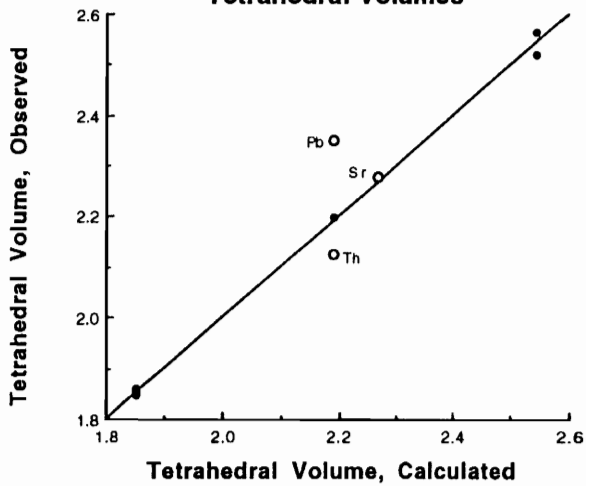

C21

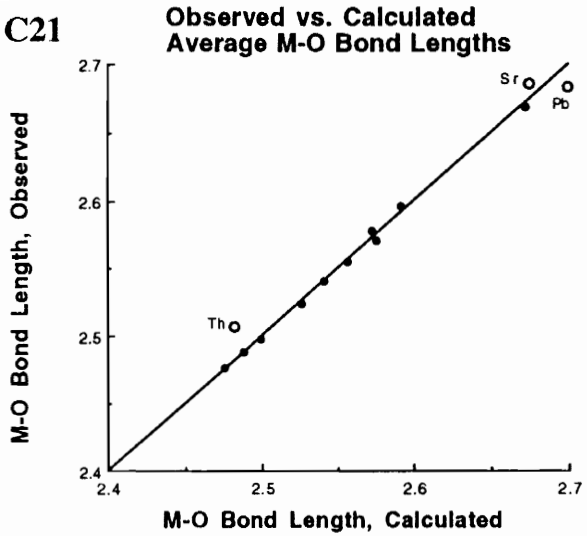

C22

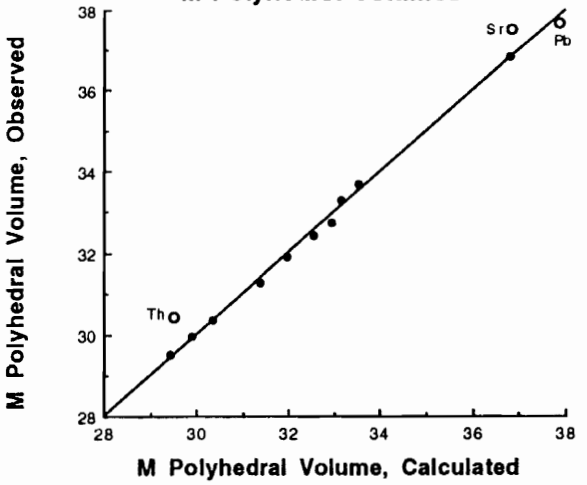

C23 Observed vs. Calculated a Cell Edge Lengths

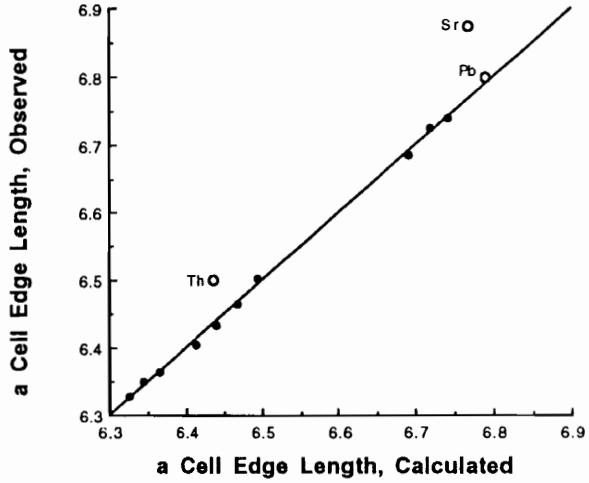

C24 Observed vs. Calculated b Cell edge Lengths

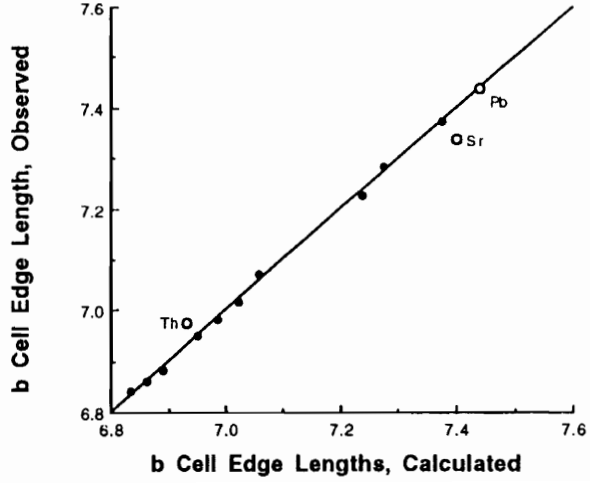

C25 Observed vs. Calculated c Cell Edge Lengths

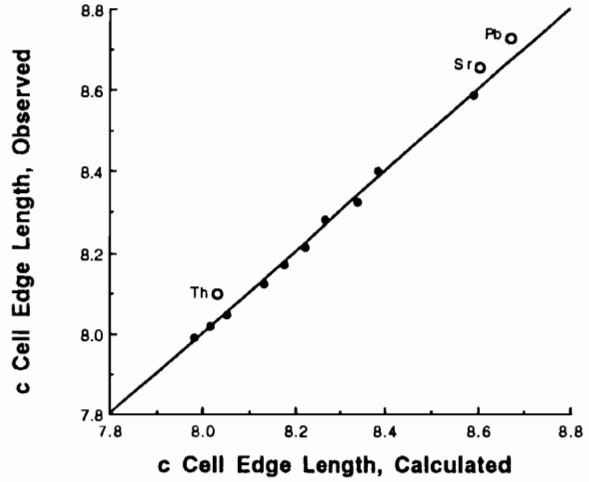

C27 Observed vs. Calculated Unit Cell Volumes

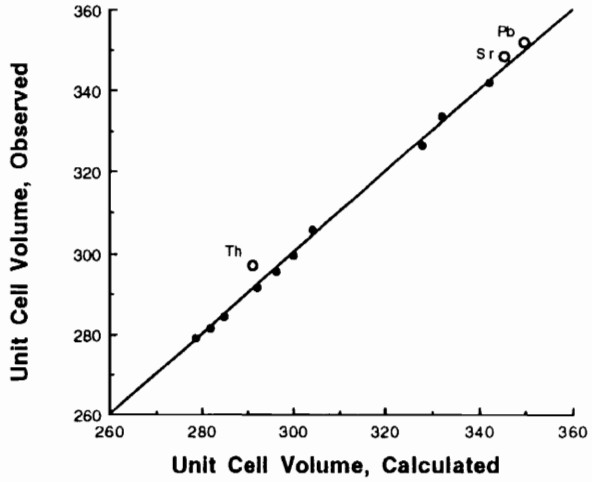

C26 Observed vs. Calculated Beta Angles

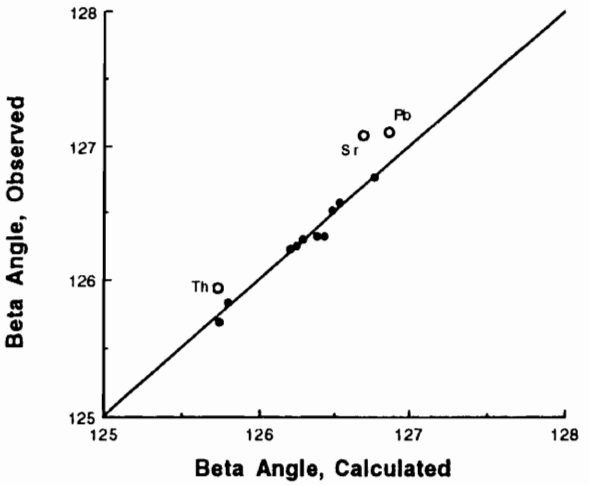

C28 Observed vs. Calculated TQE

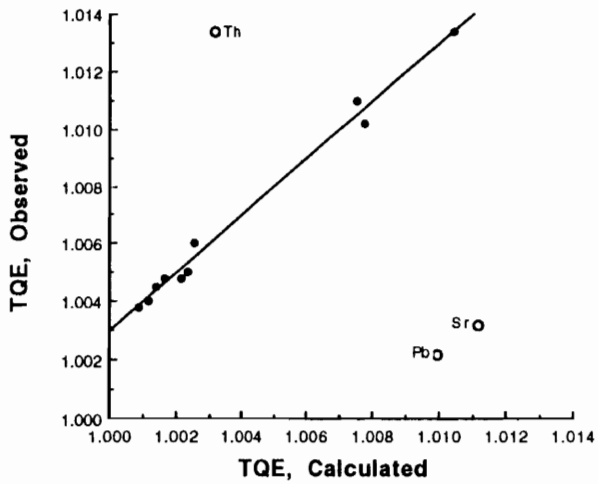

C29 Observed vs. Calculated T-O1-M1 Angles

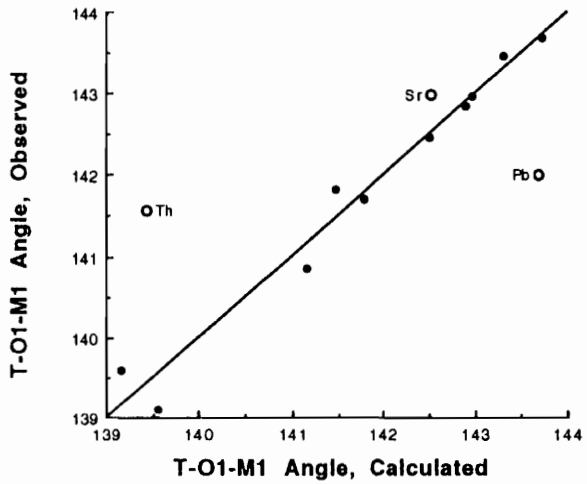

C31 Observed vs. Calculated M-O1-M Angles

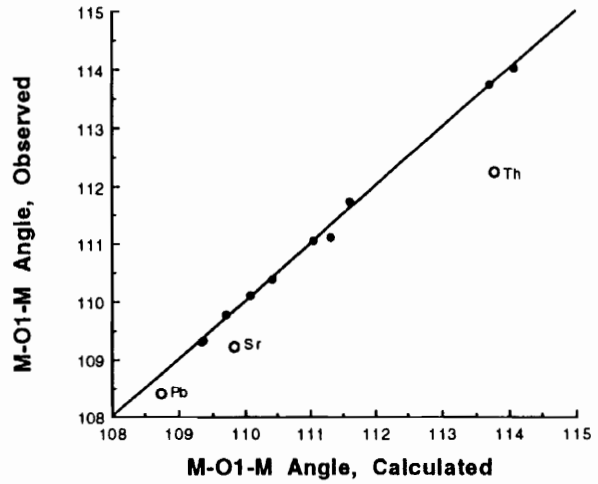

C30 Observed vs. Calculated T-O1-M2 Angles

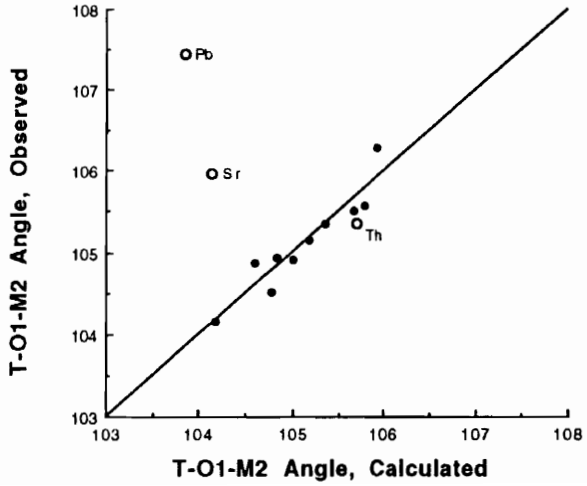

Vita

Brett Jarrod Macey was born on November 12th in 1969. Named after a T. V. character played by James Garner, his eclectic (eccentric?) interests include: heroic fantasy literature, H. P. Lovecraft, mineral collecting, heavy metal, role playing games, trading card games, and astronomy. He grew up in Spotsylvania, Virginia and now lives in Blacksburg. He has obtained his many degrees at Tech including: a B. A. in physics, a B. S. in geologic sciences, and now a M. S. in geologic sciences. He is now in the material engineering sciences program here at Virginia Tech hoping to obtain yet another degree.